Regulation of Actin Dynamics in Rapidly Moving Cells: A Quantitative Analysis

Alex Mogilner* and Leah Edelstein-Keshet†
*Department of Mathematics and Institute of Theoretical Dynamics, University of California, Davis, California 95616 USA; and
†Department of Mathematics, University of British Columbia, Vancouver, British Columbia V6T 1Z2, Canada

ABSTRACT We develop a mathematical model that describes key details of actin dynamics in protrusion associated with cell motility. The model is based on the dendritic-nucleation hypothesis for lamellipodial protrusion in nonmuscle cells such as keratocytes. We consider a set of partial differential equations for diffusion and reactions of sequestered actin complexes, nucleation, and growth by polymerization of barbed ends of actin filaments, as well as capping and depolymerization of the filaments. The mechanical aspect of protrusion is based on an elastic polymerization ratchet mechanism. An output of the model is a relationship between the protrusion velocity and the number of filament barbed ends pushing the membrane. Significantly, this relationship has a local maximum: too many barbed ends deplete the available monomer pool, too few are insufficient to generate protrusive force, so motility is stalled at either extreme. Our results suggest that to achieve rapid motility, some tuning of parameters affecting actin dynamics must be operating in the cell.

INTRODUCTION

Cell motility

Recent advances in cell biology have uncovered molecular mechanisms that control cytoskeletal dynamics underlying cell motion. The significance of such research is clear because the migration of eukaryotic cells plays a fundamental role in morphogenesis, wound healing, immune surveillance, and carcinogenesis (Bray, 1992). The crawling motion of a cell (such as a keratocyte) relies on the extension of its leading edge, the lamellipod, and requires growth of the cytoskeleton; in particular, of the actin network that is its main structural component (Tilney et al., 1991). The fact that motility is based on dynamic changes in the cytoskeleton has been known for well over a decade, but the idea that actin polymerization can, by itself, generate the force of protrusion that pushes the cell front forward (Tilney et al., 1991) was only recently confirmed quantitatively (Peskin et al., 1993; Mogilner and Oster, 1996a; Gerbal et al., 2000). This paper explores key details underlying actin-based lamellipodial protrusion using mathematical modeling. Our main goal is to understand how details of actin polymerization, nucleation, disassembly, and regulation work together in a spatially distributed way to generate and regulate protrusion of the cell front.

Cell motility is a complex, dynamic process in which cytoskeletal assembly, adhesion to extracellular matrix, and contractile forces interact in a spatially heterogeneous, complex geometry. This level of complexity has led some investigators to argue that exclusion of any one of these effects would seriously weaken the validity of a model. Nevertheless, as our main focus is on protrusion, our approach is based on the premise that it is worth investigating and understanding the biochemistry of cytoskeletal assembly as a prelude to more complex and more complete model investigations of cell motion as a whole.

To justify this approach, we temporarily put aside a longer-term goal of understanding the motility of cells such as *Dictyostelium*, fibroblasts, and leukocytes that undergo dramatic shape changes, transient and erratic locomotion, and complex, heterogeneous dynamic adhesion (Munevar et al., 2001; Beningo et al., 2001). Actin growth at the leading edge does not generally match the rate of migration: these cells have a "slippery clutch" (Theriot and Mitchison, 1992; Cameron et al., 2000). Such examples are, at present, beyond the scope of theoretical modeling as outlined in this paper and we do not attempt to model their motion in terms of actin dynamics alone. For reasons explained further (under "Choice of model system"), our main concern is with keratocyte motion. We first briefly review the relevant biological details required as a background for the model (see also Figs. 1 and 2).

The lamellipod

The basic engine of motion causing forward protrusion of the cell edge is the lamellipod (Pollard et al., 2000; Abraham et al., 1999; Small et al., 1995; Svitkina et al., 1997; Svitkina and Borisy, 1999). This structure is a broad, flat, sheet-like structure, tens of microns in width, and 0.1–0.2 μm thick (Abraham et al., 1999); see bottom panels in Fig. 1. Lamellipodial actin filaments form a highly ramified, cross-linked, polarized network; fibers subtend a roughly 55° angle with the front edge of the cell in a nearly square-lattice structure (Maly and Borisy, 2001).

Submitted March 5, 2001, and accepted for publication May 28, 2002.

Address reprint requests to Dr. Alexander Mogilner, Dept. of Mathematics, University of California-Davis, 682 Kerr Hall, Davis, CA 95616. Tel.: 530-752-1072; E-mail: mogilner@math.ucdavis.edu.

0006-3495/02/09/1237/22 $2.00

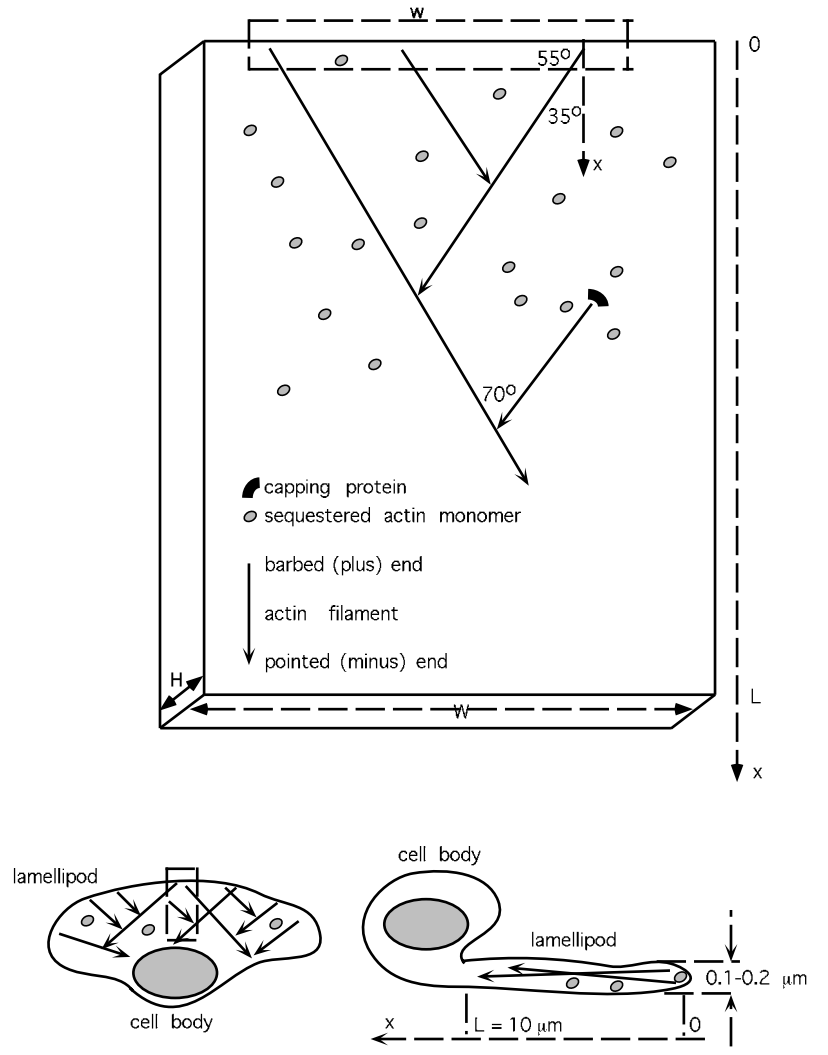

FIGURE 1 *Bottom*: A schematic diagram of a migrating fish keratocyte cell as seen from above (*bottom left*) and from the side (*bottom right*) showing typical shape and dimensions. *Top*: The rectangular portion of the lamellipod indicated in the bottom left view is here magnified, and forms region of interest for the model: its dimensions are length $L = 10$ μm, width $W \sim 1$–5 μm, and thickness $H \sim 0.1$–0.2 μm. Actin filaments are represented schematically by a few diagonal arrows. (The filaments are growing away from their pointed ends and toward the membrane at the top). The edge-density of leading barbed ends, B, is the number of barbed ends at the top surface of the box divided by w.

Actin

Actin, the major component of the lamellipodial cytoskeleton, exists in monomeric (G-actin) and rod-like polymerized filament (F-actin) forms. The actin network is regulated by a host of actin sequestering, capping, severing, nucleating, and depolymerizing proteins (Pantaloni et al., 2001; Ressad et al., 1999; Chen et al., 2000; Southwick, 2000; Machesky, 1997; Machesky and Insall, 1999; Pollard et al., 2000). There are tens to hundreds of proteins involved in actin turnover in motile cells. However, only a small number of those are essential for protrusion. The discovery of this fact (Loisel et al., 1999; Pantaloni et al., 2001) is of fundamental importance for understanding the lamellipodial dynamics. Furthermore, this makes the system amenable for modeling. Actin filaments are not homogeneous along their length. At the newly assembled end, ATP nucleotides are attached to actin; these undergo progressive hydrolysis and subsequent dissociation of the γ-phosphate over time. Nucleotide hydrolysis has been identified as the main factor determining filament half-life. Factors that accelerate filament disassembly include ADF/cofilin and gelsolin, both displaying higher affinity to the older ADP-actin sites along a filament.

Barbed ends

The ends of an actin filament have distinct polymerization kinetics, with fast-growing barbed (plus) ends directed toward the cell membrane and shrinking pointed (minus) ends directed toward the cell interior. There is evidence that most of the uncapped barbed ends are concentrated close to the cell edge, where they rapidly assemble ATP-G-actin (actin monomers with ATP attached). The *leading barbed ends* (terminology used in this paper for filament ends pushing the membrane) provide the force for protrusion. In our model we will be primarily concerned with the relationship between the number of leading barbed ends per unit length of membrane and the protrusion velocity of the cell. This

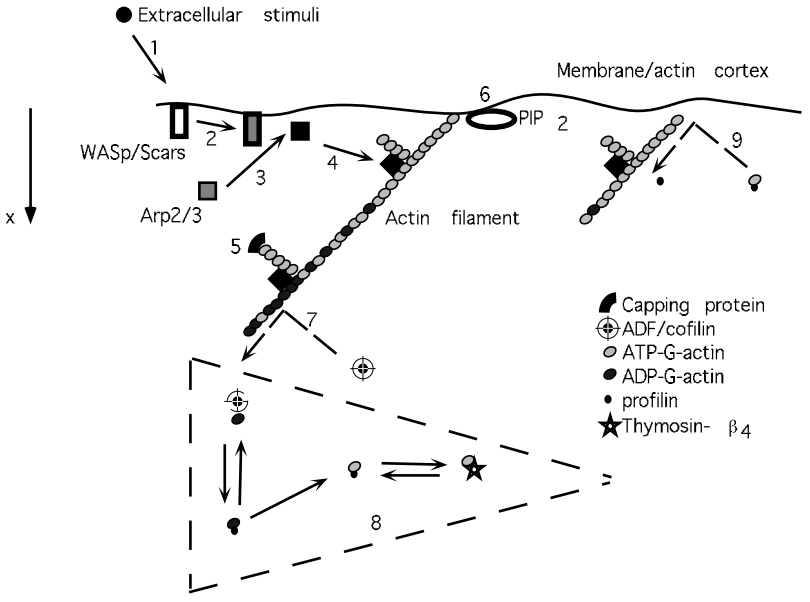

FIGURE 2 The sequence of events associated with lamellipodial protrusion based on the dendritic-nucleation model. (1, 2) Extracellular signals stimulate receptors that activate WASp/Scars; (3) WASp/Scars activate the Arp2/3 complex; (4) Arp2/3 nucleates a new actin filament barbed end by branching from some preexisting filament; (5) barbed ends of the filaments get capped in the cytoplasm; (6) PIP_2 inhibits capping at the leading edge; (7) ADF/cofilin accelerates depolymerization of actin filaments at their older, ADP-actin portions; (8) ADF/cofilin, profilin, and thymosin $\beta 4$ form complexes with G-actin, thymosin sequesters the monomers, while profilin catalyzes exchange of ADP for ATP on the actin monomers; (9) profilin-ATP-G-actin intercalates into the gap between a filament and the membrane, and assembles onto the barbed ends of actin filaments. This pushes the membrane forward.

velocity depends, among other things, on monomer availability to the growing barbed ends, a factor that must be carefully considered in understanding the mechanism. We will also be concerned with regulation of this edge-density of barbed ends by *nucleation* and *capping*.

Capping controls growth of the actin network

If polymerization were unregulated at the front edge, the pool of actin monomers would be depleted in seconds by barbed end growth. Capping of these barbed ends on the time scale of 4 s^{-1} (Pollard et al., 2000) is likely one of the main (though still not fully understood) regulatory factors (Carlier and Pantaloni, 1997). In the cytosol, uncapping is extremely slow and can be neglected on this time scale. At the leading edge, however, phosphoinositides such as PIP_2 remove barbed end caps, creating a local environment where capping is effectively reduced (Hartwig et al., 1995; Schafer et al., 1996). Barbed ends of nascent filaments close to the edge may further be protected from capping by a Cdc42-dependent mechanism (Huang et al., 1999).

Nucleation controls growth of the actin network

New barbed ends are nucleated along preexisting filaments as branches by a molecular complex, Arp2/3, known to be abundant (Kelleher et al., 1995) and essential (Schwob and Martin, 1992) for cell motility (Ma et al., 1998; Pollard et al., 2000). Under optimal conditions, each activated Arp2/3 complex initiates a new actin filament branch point (Higgs et al., 1999) at an $\sim 70°$ angle (Mullins et al., 1998); the Arp2/3 becomes integrated into the structure. It is still to be clarified whether the Arp2/3 complex binds at the side (Amann and Pollard, 2001) or at the barbed end of an actin filament (Pantaloni et al., 2000), or possibly both.

An interesting scenario of spatial and temporal self-organization in the lamellipod, called the *dendritic-nucleation model*, has been proposed (Mullins et al., 1998; Pollard et al., 2000); see Fig. 2. On a time scale of seconds (Gerisch, 1982), external signals such as chemoattractants or growth factors activate cell-surface receptors that signal a family of WASp/Scar proteins; these interact transiently with, and activate Arp2/3 complexes that can nucleate actin branching. (Blanchoin et al. 2000a; Machesky et al., 1999; Higgs and Pollard, 1999). (Indirect evidence suggests that the level of activated WASp/Scar is low relative to Arp2/3, so that activation by WASp/Scar is likely to be a limiting factor (Pollard et al., 2000).)

Signaling pathways are under current intense study (Carlier et al., 1999a, 2000; Egile et al., 1999), but it is as yet unclear whether activation occurs at the plasma membrane or in the cortical region, and exactly where branching dominates. Barbed ends have been observed mainly within 0.1 or 0.2 μm from the cell membrane, while Arp2/3 complexes appear to be more widely distributed (from the membrane up to 1.0–1.5 μm into the cell) (Bailly et al., 1999). Similarly, nucleation sites were observed in a strip <1 μm wide at the extreme leading edge (Svitkina and Borisy, 1999). Such observations suggest that activation, nucleation, and branching all occur in a narrow "activation zone" (a few hundreds of nanometers wide) at the leading edge of the lamellipod (Wear et al., 2000).

Actin monomer flux

During steady state, constant extension due to the net rate of polymerization at barbed ends of filaments has to be bal-

anced by the net rate of depolymerization at the opposite (pointed) ends. Single filaments have been noted to undergo "treadmilling" in vitro; i.e., apparent translocation by addition of monomers at the barbed end and loss at the pointed end. However, G-actin concentration would have to be two orders of magnitude greater than the in vitro treadmilling concentrations to account for the observed rates of extension (tenths of a micron per second (Pollard et al., 2000)), given the experimentally determined rate constants for actin polymerization (Pollard, 1986). Furthermore, the (slow) rate of depolymerization of the minus ends would have to increase to allow the minus ends of the filaments to keep up with the margin (Coluccio and Tilney, 1983; Wang, 1985). The actual flux of actin monomers across the lamellipod depends on rates of filament disassembly, on diffusion of these monomers in a variety of complexes, and on agents that sequester these monomers in an unusable form. Such effects are incorporated into our model.

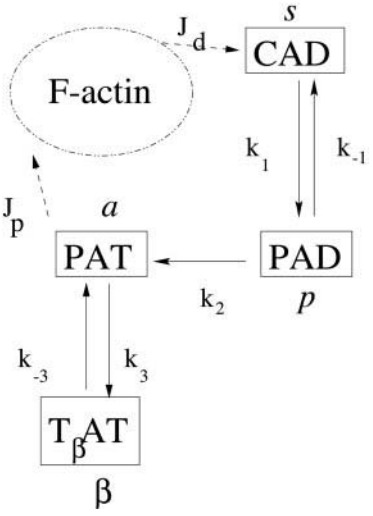

FIGURE 3 Exchange reactions for G-actin complexes of various forms: cofilin-ADP-actin (CAD), profilin-ADP-actin (PAD), profilin-ATP-actin (PAT), thymosin β4-ATP-actin (T_βAT), and filamentous actin (F-actin). The italic letters adjacent to the boxes are symbols used in the model for the concentrations of these intermediates; values of the reaction rate constants shown beside the arrows are given in Table 1.

Filament disassembly

Although filament disassembly does not appear to contribute *directly* to protrusion, it plays an important role in the recycling of monomers from rear portions of the lamellipod to the front. ATP nucleotides attached to actin undergo hydrolysis and eventual dissociation of the γ-phosphate, a process that regulates eventual disassembly of a filament. Conversion from ATP-actin to ADP-actin takes 10–30 s in rapidly migrating cells (Pollard et al., 2000). ADF/cofilin and other fragmenting proteins attach rapidly to ADP-F-actin, catalyzing dissociation of subunits from filament minus ends, or cutting filaments at ADP-actin regions (Korn et al., 1987; Pollard et al., 2000; McGrath et al., 2000). Cutting creates new minus ends and accelerates depolymerization further (Southwick, 2000).

There are several views about depolymerization: one is that each actin subunit dissociates independently from its polymer (Hill and Kirschner, 1982). The opposing vectorial hydrolysis model is that hydrolysis occurs only at the interface between ADP-P_i- and ATP-actin subunits (Carlier et al., 1986) on the filament. Recent studies provide yet a new view (Blanchoin et al., 2000b), namely that some reaction decreases the affinity of Arp2/3 to a pointed end at a branch point. Arp2/3 dissociation would then free a pointed filament end for fast "unraveling," with a cascade of rapid debranching and disassembly. This process is called *fiber-by-fiber renewal* of the whole population of filaments (Carlier et al., 1999b). This view contrasts with previously held ideas that individual fibers continually grow at their plus ends and shrink at their minus ends.

Monomer sequestering and recycling

The concentration of unpolymerized actin in a lamellipod is estimated to be lower than 100 μM (Pollard et al., 2000), but up to an order of magnitude greater than needed to account for observed rates of protrusion. A large pool of actin monomers is sequestered by actin-binding proteins in a form unavailable for polymerization; for example, in complexes with thymosin β4 and ADF/cofilin. Thymosin β4 is involved in a rapid exchange with profilin, a small protein, which also competes with ADF/cofilin for ADP-actin monomers (see Fig. 3). Profilin facilitates ADP-ATP exchange on the monomers, shifting the equilibria to ATP-G-actin-profilin complexes, which associate to barbed ends exclusively. Thus, profilin serves as a carrier between the sequestered actin monomeric pool (unavailable for polymerization) and the barbed ends of the filaments (Pantaloni and Carlier, 1993).

It is not currently feasible to experimentally measure the G-actin concentration profile (let alone the relative abundance of G-actin in various complexed forms) across the lamellipod, so there is no direct information about monomer availability at the front edge, where barbed ends are growing. However, from indirect information, including biochemical parameters governing association and dissociation of monomers with ADF/cofilin, thymosin, and profilin, and careful estimates of diffusion, and depolymerization, we can arrive at an estimate of the desired monomer profiles. This analysis forms an important contribution of this paper.

Self-organization in the lamellipod

The synergistic action of the Arp2/3 complex, capping protein, ADF/cofilin, and profilin creates a metastable state: the growing plus ends of actin filaments localize at the

extreme leading edge, the disassembling minus ends dominate away from the edge, and sequestering proteins shuttle monomers from the back to the front by simple diffusion. This mechanism replenishes monomers at the front where they are used up. Barbed-end capping produces an excess of free pointed ends. This keeps the supply of monomers plentiful and accelerates growth of any barbed ends that are temporarily uncapped, an effect termed *funneling* (Dufort and Lumsden, 1996; Carlier and Pantaloni, 1997). A summary of the pertinent phenomena is given in Fig. 7.

Choice of model cell

Some particularly simple systems involving motion based purely on actin polymerization exist biologically. One of these is the intracellular parasite, *Listeria*. Here, the connection between actin polymerization and speed of motion has been established (Marchand et al., 1995), and preliminary models have been developed for the force of propulsion (Mogilner and Oster, 1996a; Gerbal et al., 2000; Laurent et al., 1999). However, the motility of *Listeria* is not ideally suited for aspects on which we focus in this paper (though investigating *Listeria* for its own unique features would be of interest in a future treatment of this type). In *Listeria*, the role of the actin sequestering cycle is still too poorly understood for modeling to be effective. A major issue is that *Listeria* swims in a complex, biochemically heterogeneous 3D environment of the host cell. (Neither the geometry of in vitro chambers nor the biochemical milieu of cell extracts used in such chambers make the situation clearcut or simple.) This complicates a geometric treatment of the motion, but more importantly, it dissociates the tight, near-1D spatial coupling between the monomeric state of actin and the assembly of actin, a coupling that we will argue is fundamental to protrusion.

The case of keratocytes appears to be more tractable for the specific purposes we have in mind in this paper: 1) the shape of the cell is almost constant as it moves; 2) the motion is smooth and uniform. Hence the approximation of steady-state motion is quite good; 3) the geometry close to the front edge of its thin lamellipod can be approximated as one-dimensional: biochemical gradients are mainly directed along an axis pointing into the cell. (The "axis" of a *Listeria* cell is not similarly reducible to 1D, due to diffusion of monomers in its 3D environment); 4) most of the lamellipodial actin network is stationary relative to the substratum, with negligible retrograde flow (Cameron et al., 2000; Theriot and Mitchison, 1991); 5) in the steady-state mode of keratocyte movement, there is a high degree of coordination among protrusion, adhesion, and retraction, compared with other cells. For a given period of observation, spatial and temporal changes in adhesion or contractility are small so that the net effect of these other forces on the process of protrusion is nearly constant (Theriot and Mitchison, 1991; Mitchison and Cramer, 1996). This means that such confounding effects can be factored out of the model.

The above factors make it reasonable to speculate that locomotion of a keratocyte represents protrusion/treadmilling in its purest form, determined predominantly by the dynamics of actin network assembly, but see Lee and Jacobson (1997) and Oliver et al. (1999) for other opinions. It is further reasonable to conclude that the rate of migration of these cells is closely matched with the growth of actin filaments at the front edge. Indeed, as will be shown, predictions of our model for this rate of migration, based on underlying biochemistry, agree with experimentally measured cell velocity.

Goals of this paper

Several fundamental questions arise about actin-based protrusive motion: how is protrusion regulated? How many uncapped barbed ends should be kept available to grow at any given time in the cell? With too few barbed ends, it would be impossible to generate a force sufficient to drive protrusion and motion of the cell. Conversely, if there are too many growing ends, their competition for monomers would quickly deplete the pool, and this would retard growth. The goal of this paper is to understand the quantitative details of this observation within the context of the biochemical and biological parameters whose values are known. To do so, we will find it essential to address some related questions, including how monomers are distributed across the lamellipod. Specifically, we would like to estimate the optimal number of uncapped barbed ends for rapid protrusion. Another goal is to obtain a theoretical estimate of the rate of protrusion of cells under conditions of rapid steady-state motion. An important part of these goals is a comparison of theoretical estimates with experimental observations. Our model relies on the regulation of actin dynamics and treadmilling by a small host of essential proteins (Loisel et al., 1999; Pantaloni et al., 2001).

The model introduced in the next section is an initial attempt to elucidate general principles of spatial and temporal regulation of actin pools in the cell and determine how actin dynamics optimal for protrusion can be achieved. We will describe the dynamics of actin and of its essential associated proteins by a system of reaction-diffusion-advection equations. A sketch of the analysis of our model is provided in the following section (with further details in the Appendix). Complemented with the force-velocity relation for actin filaments, these equations will reveal the way that the protrusive rate of motion depends on key biochemical parameters and on membrane tension (Results). Biological implications of the model will be discussed in the last section.

TABLE 1 Model parameters

Symbol	Value	Meaning	Reference
δ	2.2 nm	Filament length increment per monomer	Estimated in this paper
L	$\simeq$10 μm	Length of lamellipod	Svitkina et al., 1997a
k_{on}	11.6 μM^{-1} s^{-1}	Barbed-end monomer assembly rate constant	Pollard, 1986
γ	$\sim$1 s^{-1}	Barbed end capping rate at leading edge	Pollard et al., 2000
n	$\sim$100 μm^{-1} s^{-1}	Nucleation rate	Estimated in this paper
D	30 μm^2 s^{-1}	Diffusion coefficient of G-actin complexes	Abraham et al., 1999; see Appendix
k_1	2 s^{-1}	CAD $\rightarrow$ PAD reaction rate: see Fig 3	Estimated in Appendix
k_{-1}	10 s^{-1}	PAD $\rightarrow$ CAD reaction rate: see Fig 3	Estimated in Appendix
k_2	20 s^{-1}	PAD $\rightarrow$ PAT reaction rate: see Fig 3	Estimated in Appendix
k_3	2 s^{-1}	PAT $\rightarrow$ T_βAT reaction rate: see Fig 3	Estimated in Appendix
k_{-3}	2 s^{-1}	T_βAT $\rightarrow$ PAT reaction rate: see Fig 3	Estimated in Appendix
η	100 μM^{-1} μm^{-2}	Conversion factor	Estimated in Appendix
F	$\sim$100 pN μm^{-1}	Membrane resistance force per unit edge length	Dai et al., 1998; Dai and Sheetz, 1999; Raucher and Sheetz, 1999; Erickson, 1980; Petersen et al., 1982
k_BT	$\simeq$4.1 pN $\cdot$ nm	Thermal energy	Peskin et al., 1993
A	$\sim$250 μM	Total lamellipodial actin concentration	Pollard et al., 2000
r	$\sim$1/(30 s)	Effective rate of actin filament disassembly	Pollard et al., 2000

DESCRIPTION OF THE MODEL

The meanings and values for rates and parameters in the model are given in Table 1. A list of the main variables and their definitions is given below.

- t time (s);
- x distance from the leading edge (μm);
- $B(t)$ edge density of the uncapped leading barbed ends (μm^{-1});
- $s(x, t)$ density of ADP-G-actin sequestered by ADF/cofilin (μM);
- $p(x, t)$ density of ADP-G-actin-profilin complexes (μM);
- $a(x, t)$ density of ATP-G-actin-profilin complexes (μM);
- $\beta(x, t)$ density of ATP-G-actin-thymosin β4 complexes (μM);
- $f(x, t)$ length density of F-actin ($\mu m/\mu m^2$);
- $m(x, t)$ density of uncapped minus ends (μm^{-2});
- $m_c(x, t)$ density of capped minus ends (μm^{-2});
- V protrusion velocity ($\mu m\ s^{-1}$).

Geometry of the model

We neglect curvature of the lamellipodial leading edge and any variation in the actin density in a direction parallel to the cell front or across the thickness of the sheet. In the case of the broad fan-like, thin lamellipod of keratocytes, this approximation is an excellent one. This idealization allows us to consider a 1D model, and greatly increases mathematical tractability. We assume very strong adhesion, and, as a consequence, no slippage at the cell front. This assumption is supported by observations of the rapidly moving keratocytes (Theriot and Mitchison, 1991).

We consider a thin strip of lamellipod perpendicular to the cell edge (see rectangular box in Fig. 1). We use a coordinate system moving with the front edge of the cell: our x axis will coincide with the length of the strip with $x = 0$ at the leading edge, and x representing the distance into the cell. The length of the lamellipod, L, is a model parameter. We define a barbed end "edge density," $B(t)$, as the number of uncapped leading barbed ends at $x = 0$ per unit edge-length (see Fig. 7). These leading barbed ends do the work of pushing the membrane. Concentrations of actin and actin-associated proteins are in micromoles. All densities and concentrations vary with time t and position x.

As a simplification for modeling purposes, we assume a perfect angular order in the actin network, with each filament oriented at $\pm 35°$ relative to the direction of motion of the cell. (A 70° angle between branching filaments and a flat edge implies that each filament subtends an acute angle of $\pm 55°$ at the leading edge. The observed angular distribution of the lamellipodial F-actin supports our approximation (Maly and Borisy, 2001).) When a monomer of size 5.4 nm adds onto the tip of a filament oriented in this way, the tip advances by roughly $\delta = (5.4/2) \cdot \cos(35°) \simeq 2.2$ nm along our chosen x axis. (The factor (1/2) stems from the fact that polymerized actin forms a double helix.)

The differential equations of the model are derived below. Figs. 1, 3, and 7 help capture the geometry, notation, and basic assumptions of the model. Because our coordinate system is moving with the edge of the cell (whose velocity in the absence of slippage is the protrusion rate V), most equations contain terms of the form Vdc/dx, where c is some concentration or density. This is simply a transformation to the moving coordinate system, which keeps the leading edge at the origin.

Barbed ends

The density of the barbed ends is governed by the following equation:

$$\frac{dB}{dt} = n - \gamma B. \tag{1}$$

The first term in the right-hand side of this equation represents a rate of initiation of new barbed ends (branching) by Arp2/3 with the rate n [s^{-1} μm^{-1}] at the leading edge. Actin branching takes place within the "activation zone." The barbed ends nucleated within this zone grow rapidly toward the cell membrane, where the growth is stalled significantly by membrane resistance. This creates a steep gradient of barbed end density from a high level at the leading edge down to zero at the rear of the activation zone. We assume that the width of this zone is small (much smaller than all other spatial scales inherent to the process). This allows us to treat the uncapped barbed end density as an essentially 1D "edge density," defined as the number of ends per unit length of the leading edge, rather than the number per unit area in the lamellipod.

The last term in Eq. 1 represents loss of barbed ends due to capping at rate γ. The rates of nucleation and capping in Eq. 1 are assumed to be constant model parameters. This simplification is based on the assumption that the level of activated Arp2/3 is a limiting factor, and that branching sites on preexisting filaments are in abundant supply. Furthermore, we also assume that activation by WASP (rather than the level of Arp2/3) is the rate-limiting step that determines the level of activated Arp2/3 complexes available for branching. (We thus justify the simplification in which full dynamics of Arp2/3 can be omitted.) These assumptions and the constant effective capping rate are discussed in the last section.

Monomer recycling and exchange

We assume that almost all of the G-actin in the lamellipod occurs in complexes with one of three essential sequestering proteins, ADF/cofilin, profilin, or thymosin β4. Residual free ATP-G-actin certainly occurs, as in its absence, ATP-G-actin-profilin concentration would decay to zero. Actin-based movement of pathogenic bacteria is possible without profilin, through assembly of ATP-G-actin (Loisel et al., 1999). However, we demonstrate in the Appendix that in the presence of large amounts of profilin the steady-state concentration of ATP-G-actin is very small, and ATP-G-actin-profilin is the main species polymerizing at the barbed ends. (This theoretical conclusion has been established experimentally in Pantaloni and Carlier, 1993.) We show that at observed high concentrations of profilin and thymosin (Pollard et al., 2000), ATP-G-actin concentration adjusts rapidly to the level determined by the slowly varying concentrations of G-actin in sequestered forms. Mathematically, this means that on time scales characteristic to the processes described by the model, ATP-G-actin concentration can be expressed as a function of the sequestered actin concentrations.

The following equations account for actin monomers in the forms ADP-G-actin-ADF/cofilin (s), ADP-G-actin-profilin (p), ATP-G-actin-profilin (a), and ATP-G-actin-thymosin β4 (β) complexes (see Figs. 3 and 7):

$$\frac{\partial s}{\partial t} = -V\frac{\partial s}{\partial x} + D\frac{\partial^2 s}{\partial x^2} - k_1 s + k_{-1} p + J_d(x), \tag{2}$$

$$\frac{\partial p}{\partial t} = -V\frac{\partial p}{\partial x} + D\frac{\partial^2 p}{\partial x^2} + k_1 s - k_{-1} p - k_2 p, \tag{3}$$

$$\frac{\partial \beta}{\partial t} = -V\frac{\partial \beta}{\partial x} + D\frac{\partial^2 \beta}{\partial x^2} - k_{-3}\beta + k_3 a, \tag{4}$$

$$\frac{\partial a}{\partial t} = -V\frac{\partial a}{\partial x} + D\frac{\partial^2 a}{\partial x^2} + k_{-3}\beta - k_3 a + k_2 p. \tag{5}$$

Above, we have captured the dynamics of ADP-G-actin sequestered by cofilin and profilin (Eqs. 2 and 3, respectively), and ATP-G-actin sequestered by thymosin β4 and profilin (Eqs. 4 and 5). Terms of the form Vdc/dx in the equations stem from the moving coordinate system and second derivative terms represent simple molecular diffusion. Sequestering agents are small molecules, and hence their complexes with actin share roughly similar diffusion coefficients, denoted by D: see the Appendix.

In Eq. 2 the term $J_d(x)$ depicts the distribution of sources of ADP-G-actin-cofilin from depolymerization of filaments. All other terms in these equations represent rates of exchange of actin between its sequestering agents and between the ADP-G-actin and ATP-G-actin forms as shown in Fig. 3. For example, the terms $\pm k_2 p$ describe ADP-ATP exchange on profilin-actin complexes. In the Appendix we provide estimates for the associated reaction rate constants.

We assume that the variables s, p, and β, satisfy no-flux boundary conditions at the leading edge, $x = 0$, and at the base of the lamellipod, $x = L$. However, because ATP-actin-profilin complexes are used up at the leading edge in the course of the polymerization of the filaments abutting the cell membrane, the appropriate boundary condition at $x = 0$ for $a(x, t)$ is a given flux of these complexes:

$$\left(-D\frac{\partial a}{\partial x} + Va\right)\Big|_{x=0} = -J_p = -VB/\delta\eta. \tag{6}$$

Here $(-D\partial a/\partial x(0) + Va(0))$ is the sum of diffusive and convective fluxes of ATP-actin-profilin complexes at the leading edge. This flux is directed out of the cytoplasm, in the direction of motion, and therefore carries a negative sign ($-J_p < 0$). The magnitude of this flux, J_p, is given by the rate of monomer addition per filament, V/δ ([s^{-1}]), multiplied by the density of leading uncapped barbed ends that are growing and using up monomers at the membrane, B.

The factor $1/\eta$ converts the flux into suitable dimensions: [μm^{-1} s^{-1}] into [$\mu M \cdot \mu m$ s^{-1}]. ($\eta \simeq 100$ μM^{-1} μm^{-2} is a constant, converting concentrations from μM to number of monomers per μm^2 in the fixed-thickness lamellipod; see Appendix.) We assume that the variable a satisfies no-flux boundary conditions at the base of the lamellipod, $x = L$.

Depolymerization

The G-actin distribution depends on a function to be specified, namely the source $J_d(x)$ of ADP-G-actin-ADF/cofilin disassembling from F-actin. We can only speculate about the form of $J_d(x)$ because, as discussed in the Introduction, details of depolymerization are not yet well understood biologically. We will consider a specific source function in the framework of the array treadmilling model (Svitkina and Borisy, 1999).

Debranching (or "pruning") of actin filaments may occur by spontaneous dissociation or by ADF/cofilin-induced dissociation of Arp2/3 from a Y-junction in the actin network. Each such event creates an uncapped minus end. Here, the filament begins to unravel, producing a source of ADP-G-actin-ADF/cofilin until disassembly is complete. The dynamics of the minus ends (density $m(x, t)$), and those still capped by Arp2/3 (density $m_c(x, t)$), can be described by the following equations:

$$\frac{\partial m_c}{\partial t} = -V\frac{\partial m_c}{\partial x} - \frac{m_c}{t_1}, \tag{7}$$

$$\frac{\partial m}{\partial t} = -V\frac{\partial m}{\partial x} + \frac{m_c}{t_1} - \frac{m}{t_2}. \tag{8}$$

Spatial derivative terms arise from the moving coordinate system. Terms proportional to m_c describe uncapping of the minus ends. We assume that uncapping is a slow Poisson process characterized by rate $1/t_1 \sim 30$ s. A term proportional to m accounts for elimination of uncapped minus ends due to complete disassembly of a filament. The average filament lifetime, t_2, depends on the average filament length, l, and on the rate of depolymerization of the filaments, V_{dep}. The former can be estimated as the ratio of filament growth rate to filament capping rate: $l \approx V/\gamma$. (Using the observed $V \sim 0.5$ μm s^{-1} and $\gamma \sim 4$ s^{-1}, we obtain $l = V/\gamma \sim 0.1$ μm.) The effective rate of depolymerization of ADF/cofilin-F-actin from the minus end is unknown, but a convincing theoretical argument (Carlier et al., 1999b) suggests that its order of magnitude is $V_{dep} \sim 0.1$ μm s^{-1}. Combining these estimates, we arrive at the approximation $t_2 = l/V_{dep} \sim 1$ s.

Equations 7 and 8 must be supplemented with appropriate boundary conditions. We use the fact that Arp2/3-capped minus ends are nucleated at the front simultaneously with barbed ends, i.e., at the same rate, n. Thus, the density of the Arp2/3-capped minus ends at the leading edge, $m_c(0)$, is equal to the nucleation rate divided by the speed of the lamellipodial front. Assuming all minus ends at the leading edge are capped then leads to the boundary conditions:

$$m_c(0) = \frac{n}{V}, \quad m(0) = 0. \tag{9}$$

The G-actin source $J_d(x, t)$ is proportional to the density of uncapped minus ends:

$$J_d(x, t) = \frac{V_{dep}}{\delta\eta} m(x, t). \tag{10}$$

Factor $1/\eta$ converts the dimension of the source term into [μM s^{-1}].

Clearly, this model of depolymerization is grossly simplified. There may be many other mechanisms acting to liberate actin monomers. In the Appendix, we discuss the feasibility of the alternative tread-severing model (Dufort and Lumsden, 1996). Also, at the rear of the lamellipod, myosin-generated contraction (Svitkina et al., 1997) physically breaks actin fibers, creating many minus ends and massive depolymerization. Recent information points to the involvement of tropomyosin and other actin-associated proteins in regulating F-actin stabilization. Furthermore, there is a pronounced difference between the highly branched actin meshwork seen at the front and the smoother network further into the lamellipod (Blanchoin et al., 2001). This may indicate that the rates of debranching and/or severing vary significantly from one region in the lamellipod to another.

Protrusion velocity

If not for the membrane resistance and depolymerization, the barbed ends at the leading edge would grow with the free polymerization velocity:

$$V_0 = k_{on}\delta a(0). \tag{11}$$

Here, k_{on} [s^{-1} μM^{-1}] is the rate constant for monomer assembly, $a(0)$ [μM] is the concentration of ATP-G-actin-profilin complexes at the front, and $k_{on}a(0)$ is the local rate of assembly of monomers per unit time at the barbed end of a filament. Multiplied by δ, the length increment due to the addition of a single monomer, this rate becomes the free polymerization velocity.

The cell membrane associated with the actin cortex imposes a resistance to the propulsive motion. Because of this resistance, the velocity of protrusion, V, is smaller than the free polymerization velocity, V_0. We require a relationship between the resistance force per unit length of the leading edge, F [pN/μm], and the protrusion velocity $V = V(V_0, F)$, to close the system of equations forming our model. However, as no measurements are currently available for this force-velocity relation in actin-based lamellipodial protrusions, here we must rely on theoretical arguments for the desired formula. Peskin et

al. (1993) and Mogilner and Oster (1996a) derived expressions for the force-velocity relation for a single actin filament growing against a given load force, f. In the limiting case when bending undulations of the filaments and the cell membrane are much faster than polymerization kinetics, and when the average amplitude of such undulations is greater than the size of an actin monomer, the relationship has the form:

$$V = \delta(k_{on}a(0)e^{-\delta f/k_B T} - k_{off}),$$

where k_{on} and k_{off} are the polymerization and depolymerization rate constants, respectively, T is absolute temperature, and k_B is Boltzmann's constant.

Although this is a limiting case, it adequately describes most biological situations based on physiological values of the parameters associated with filament and membrane mechanics and actin concentrations in the cell (Mogilner and Oster, 1996a; Mogilner and Oster, 1999). For fast-moving cells, the rate of depolymerization of actin from barbed ends, k_{off}, is negligible, so that the force-velocity relation is well approximated by

$$V \simeq V_0 e^{-\delta f/k_B T}.$$

That is, the free polymerization rate, V_0, is weighted by a Boltzmann factor, where the exponent, $\delta f/k_B T$, is the work (in units of thermal energy, $k_B T \simeq 4.1$ pN · nm) done against the load by the assembly of one monomer. Note that near stall, when resistance is high, viscous dissipation can be neglected, the work of polymerization is almost reversible, and the above force-velocity relation follows from general thermodynamical arguments that do not depend on a detailed microscopic model (Hill, 1987).

To now apply this relation to a *population* of filaments, $B(t)$ pushing against the membrane load, we take the simplest and most easily justifiable assumption; namely, that the load is equally divided among the filaments, each bearing a share $f = F/B$ (Mogilner et al., 2001; van Doorn et al., 2000). The resulting form of the load-velocity relation for the lamellipodial front is:

$$V = V_0 \exp(-w/B), \quad w = F\delta/k_B T. \tag{12}$$

We will assume this relationship henceforth.

In Eq. 12, values of the constants δ, k_B, and T are known, but we require estimates for the resistance force, F. Two factors contribute to this force. The first is membrane surface tension with bending modulus determined by the splay of the outer membrane leaflet and compression of the inner leaflet (Evans and Skalak, 1980). The second is binding energy dissipation when the links between the actin cortex and membrane are broken as the membrane is pushed forward. The value of the total resistance force can be estimated to be $F \sim 50$–500 pN/μm (Dai et al., 1998; Dai and Sheetz, 1999; Raucher and Sheetz, 1999; Erickson, 1980; Petersen et al., 1982). In this paper we will use the value $F = 100$ pN/μm for the estimates. The velocity dependence of the resistance force is very weak (Hochmuth et al., 1996).

Gerbal et al. (2000) developed a different, mesoscopic model relying on the elastic shear stress generation due to the growth of the actin gel. They demonstrated that the rate of growth of the actin meshwork is decreased (in comparison with the velocity given by formula (12) due to elastic recoil under load by a factor on the order of $(1 + (F/YH))$, where Y is the Young modulus of the lamellipodial cytoskeleton and H is the thickness of the lamellipod. In the physiological range of the resistance load, this effect does not introduce a significant correction to Eq. 12 because the lamellipodial network is very stiff: $Y \sim 10^4$ Pa (Rotsch et al., 1998), and $F/YH < 0.2$.

ANALYSIS OF THE MODEL

Spatial distribution of uncapped barbed ends

The stationary solution for the density of uncapped barbed ends at the leading edge can be found from Eq. 1:

$$B = \frac{n}{\gamma}. \tag{13}$$

The distribution of actin monomers

A first important observation concerns the relative magnitudes of the diffusion and drift terms in Eqs. 2–5. In the Appendix we demonstrate that diffusion of the G-actin complexes is much faster than drift on a spatial scale relevant for the lamellipod. This justifies neglecting the drift terms in Eqs. 2–5 for our purposes.

These approximations lead us to the following simplified system for the stationary distribution of sequestered monomers:

$$D\frac{d^2 s}{dx^2} - k_1 s + k_{-1} p + J_d(x) = 0$$

$$\left.\frac{ds}{dx}\right|_{x=0} = \left.\frac{ds}{dx}\right|_{x=L} = 0 \tag{14}$$

$$D\frac{d^2 p}{dx^2} + k_1 s - k_{-1} p - k_2 p = 0$$

$$\left.\frac{dp}{dx}\right|_{x=0} = \left.\frac{dp}{dx}\right|_{x=L} = 0 \tag{15}$$

$$D\frac{d^2 \beta}{dx^2} - k_{-3}\beta + k_3 a = 0$$

$$\left.\frac{d\beta}{dx}\right|_{x=0} = \left.\frac{d\beta}{dx}\right|_{x=L} = 0 \tag{16}$$

$$D\frac{d^2 a}{dx^2} + k_{-3}\beta - k_3 a + k_2 p = 0$$

$$\left.\frac{da}{dx}\right|_{x=L} = 0, \left.\frac{da}{dx}\right|_{x=0} = \frac{J_p}{D} \tag{17}$$

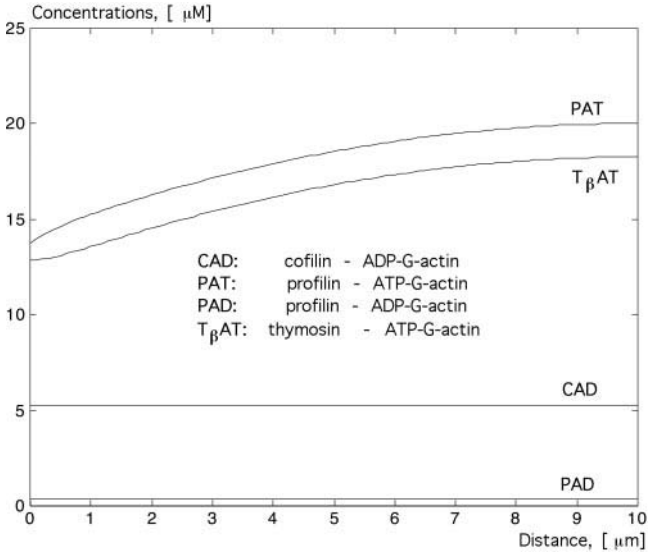

FIGURE 4 Stationary concentrations of sequestered G-actin complexes are plotted (using formulae (22, 33, 34) for values of the model parameters listed in Table 1) as functions of distance from the front edge of the cell. The concentrations of ADP-G-actin bound to profilin (PAD) and ADF/cofilin (CAD), 0.35–5 μM, respectively, are constant over the lamellipod. Concentrations of ATP-G-actin complexes with profilin (PAT) or thymosin ($T_\beta AT$) decrease from the rear to the front of the lamellipod.

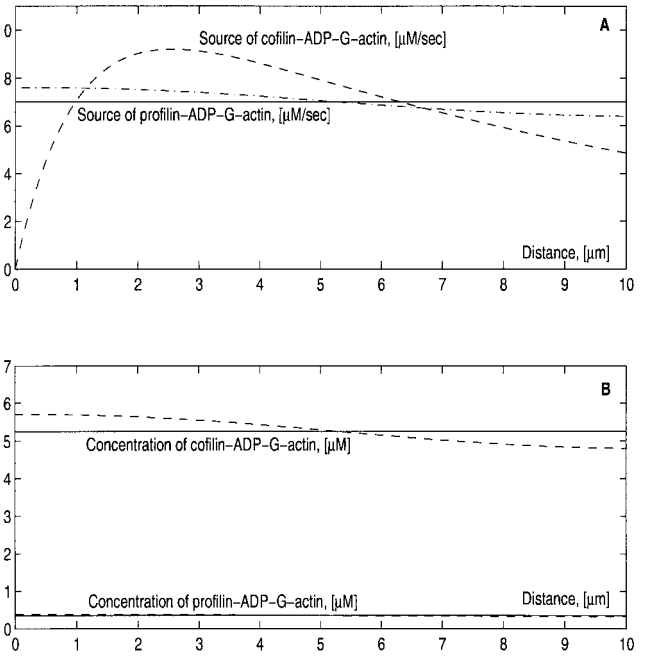

FIGURE 5 (*A*) Distribution of the source of cofilin-ADP-actin as given by treadmilling model (*dashed line*) and corresponding distribution of the source of profilin-ADP-actin obtained numerically (*dot-dashed line*). The solid line is an approximate constant source of profilin-ADP-actin. (*B*) Concentrations of cofilin- and profilin-ADP-actin. The dashed curves represent the numerically computed concentrations. The solid lines are approximate constant concentrations.

We now comment on the behavior of the solution to this system, below (see Fig. 4 for a plot of the results).

The depolymerization source

The linear equations of the array treadmilling model (7–10) can be solved analytically (see the Appendix). The corresponding steady-state solutions for the number of free and capped minus ends of filaments have the following forms:

$$m_c(x) = \frac{n}{V}\exp\left(-\frac{1}{Vt_1}x\right), \tag{18}$$

$$m(x) \simeq \frac{n}{V}\frac{t_2}{t_1}\left[\exp\left(-\frac{1}{Vt_1}x\right) - \exp\left(-\frac{1}{Vt_2}x\right)\right]. \tag{19}$$

The model predicts that the density of uncapped pointed ends builds up exponentially away from the leading edge up to a certain distance from the front, and then decays exponentially toward the rear (see Fig. 5). The model is characterized by two distinct spatial scales. A short spatial scale on the order of 1 μm corresponding to Vt_2 captures the average protrusion distance of the leading edge during the time it takes for an actin filament to disassemble completely from an uncapped minus end. The depolymerization source attains a maximum at roughly this distance away from the leading edge. A long spatial scale on the order of 10 μm corresponding to Vt_1 is set by the average distance of protrusion that occurs over the time it takes for a new uncapped minus end to be created. This corresponds to the spatial scale on which F-actin density is decreased. Note that experimentally, a 9% decrease of F-actin density is observed per 1 μm distance from the leading edge (Pollard et al., 2000): this implies a length scale of $\ell \sim 10$ μm for significant changes in actin density (as approximated by a simple exponential decay $\exp(-x/\ell)$). This matches our estimate well.

The total number of uncapped pointed ends can be estimated by integrating the expressions for $m(x)$ across the length of the lamellipod (from 0 to L). This leads to an estimate on the order of 1000 (per rectangle of dimensions 1 μm $\times$ 10 μm at the leading edge). The number of uncapped barbed ends at the front is on the order of 100 per 1 μm (see below). Thus, the predicted ratio of the number of uncapped minus and plus ends, $\sim$10, turns out to match the estimate in Carlier and Pantaloni (1997) and *our estimates support a funneling model* (Dufort and Lumsden, 1996; Carlier and Pantaloni, 1997).

The model leads to an expression for the distribution of the G-actin source. The following formula can be derived using Eqs. 10, 19, and 32:

$$J_d(x) \simeq J(e^{-x/l} - e^{-x/\tilde{l}}), \quad l \simeq 10\ \mu\text{m},$$

$$\tilde{l} \simeq 1\ \mu\text{m}, \quad J \simeq \frac{P}{t_1}, \tag{20}$$

where P is the average F-actin concentration.

ADP-G-actin

Equations 14 and 15 are independent of the variables a and β, and can be treated in isolation. Any attempt at analytical solution of these equations with the distribution of the G-actin source (20) is very cumbersome and does not provide biological insight. However, numerical experimentation with Eqs. 14 and 15 and 20 leads to a fortuitously convenient observation: even though the source distribution of depolymerizing actin has significant inhomogeneities, the steady-state distribution of ADP-G-actin-profilin is nearly uniform. We found that the profile of ADP-G-actin-profilin deviates only very slightly, $\pm 10\%$, from some average value, as shown in Fig. 5. We attribute this fact to the smoothing effect of diffusion occurring over the time of G-actin exchange between ADF/cofilin and profilin.

This numerical observation is fortunate, as it allows us to approximate the source term $J_d(x)$ by a constant:

$$J_d(x) \simeq J = rP = \text{const.} \tag{21}$$

Here, $r = 1/t_1 \sim 1/30\ \text{s}^{-1}$ (Pollard et al., 2000) is the effective F-actin disassembly rate. Essentially, this is the rate of minus ends uncapping or severing, because disassembly is relatively fast once this occurs. The average depolymerization source is rP, where P is the average F-actin concentration. If $P \simeq 210\ \mu\text{M}$, then $J \simeq 7\ \mu\text{M s}^{-1}$. Assuming (21) greatly simplifies analysis, because exact solutions of Eqs. 14 and 15 with constant $J_d(x) = J$ are uniform. When no-flux boundary conditions are applied, we find that $s(x)$ and $p(x)$ are constants given by:

$$s(x) = s = \frac{k_{-1} + k_2}{k_1 k_2} J, \quad p(x) = p = \frac{J}{k_2}. \tag{22}$$

The term $(k_2 p)$ in Eq. 17 now becomes a constant source term, J.

Observations of fluorescence dissipation after photoactivation (Theriot and Mitchison, 1991) were interpreted to mean that depolymerization occurs uniformly within the lamellipod, supporting this approximation. Similar conclusions have been based on observations of the comet tails of *L. monocytogenes* (Theriot et al., 1992; Rosenblatt et al., 1997). We discuss possible modifications of the model results due to the more complex realistic situation with depolymerization in vivo below.

ATP-G-actin

We are now left with the equations

$$D \frac{d^2\beta}{dx^2} - k_{-3}\beta + k_3 a = 0$$

$$D \frac{d^2 a}{dx^2} + k_{-3}\beta - k_3 a + J = 0,$$

for thymosin-actin and profilin-actin, together with the boundary conditions

$$\frac{da}{dx}(0) = J_p/D$$

$$\frac{da}{dx}(L) = \frac{d\beta}{dx}(0) = \frac{d\beta}{dx}(0) = 0.$$

A stationary state can be achieved only when the total depolymerization flux, JL, is equal to the polymerization flux, J_p. This leads to the condition $J_p = JL$, required for consistency (see the Appendix). Furthermore, the solution depends on the total concentration of actin (in all its forms) in the lamellipod, denoted by A [μM] and on the expression for the depolymerization flux (21).

The above system forms a set of linear fourth-order differential equations. Together with the four boundary conditions, these specify a unique solution for $a(x)$ and $\beta(x)$. Explicit expressions for these stationary concentrations of sequestered ATP-G-actin are given in the Appendix (Eqs. 33 and 34) and shapes of the spatial profiles are shown in Fig. 4. The concentrations of ATP-G-actin complexed with thymosin and profilin (PAT and T_βAT) are lowest at the front edge due to depletion by polymerization there. Other intermediates, such as ADP-G-actin complexed with cofilin and profilin (CAD and PAD) are constant across the region.

The expression (33) for ATP-G-actin can now be evaluated at $x = 0$ to find the concentration of polymerization-competent actin at the leading edge. This is the result of interest for our model: the concentration of *available* G-actin at the leading edge is the single most important factor determining the rate of polymerization and growth of the actin network. We obtain:

$$a(0) = \frac{k_{-3}}{k_3 + k_{-3}} \left(A - \frac{J_p \tau}{L} \right), \tag{23}$$

where

$$\tau = \tau_{dep} + \tau_{cof} + \tau_{rec}, \quad \tau_{dep} = 1/r,$$

$$\tau_{cof} = \frac{k_1 + k_{-1} + k_2}{k_1 k_2},$$

$$\tau_{rec} = \frac{L^2}{3D} + \frac{k_3}{k_{-3}(k_3 + k_{-3})} \left[\sqrt{\frac{L^2(k_3 + k_{-3})}{D}} - 1 \right]. \tag{24}$$

We can understand the meaning of expression 23 for the available G-actin as follows: the factor $k_{-3}/(k_3 + k_{-3})$ represents partitioning between sequestered thymosin-actin and available profilin-actin. The negative term $(-J_p\tau/L)$ subtracts the portion unavailable for polymerization from the total concentration of actin, A. We observe that the effect of this term gets larger when the polymerization flux depleting ATP-G-actin, J_p, increases, or when the parameter τ (described below) increases.

The parameter τ can be interpreted as the *actin monomer turnover time*. Then, L/τ is the effective rate of transport (in units of speed) of actin in a form unavailable for polymerization through the lamellipod, and $J_p/(L/\tau)$ is the concentration of this unavailable actin. Furthermore, τ_{dep} corresponds to a depolymerization time and τ_{cof} to a time of ADP-ATP exchange on G-actin. Further, τ_{rec} represents the time it takes to recycle monomers from the cytoplasm to the leading edge and their conversion into the polymerization-competent state. This recycling time is essentially the diffusion time across the lamellipod, $\sim L^2/D$, scaled by a factor representing dynamic exchange between profilin and thymosin.

For rapidly moving cells (with model parameters of Table 1), typical values of these times are $\tau_{dep} = 1/r \sim 30$ s, while $\tau_{cof} < 1$ s and $\tau_{rec} \sim 1$–2 s. This means that the polymer disassembly time is much longer than the ADP-ATP exchange and recycling time, so depolymerization is rate-limiting.

This situation can change due to any of the following factors. The effective diffusion coefficient may decrease (to as low as 5–10 $\mu m^2\ s^{-1}$) if filaments in the cytoskeleton are crowded together too tightly. Furthermore, if the length of the lamellipod also doubles, then our estimate for the recycling time increases to $\tau_{rec} \sim 20$ s, becoming comparable to the depolymerization time. Alternatively, F-actin disassembly might be regulated spatially in a way other than the one assumed in this paper; for example, it might be taking place at the rear of the cell (Abraham et al., 1999; Olbris and Herzfeld, 1997). For such situations, analysis similar to the one performed here reveals that both Eq. 23 and the expression for τ (in terms of the sum of the depolymerization, exchange and recycling times) still hold. However, the values of each of these times change, in some cases significantly.

Protrusion velocity and leading barbed ends

Equation 23 linking actin monomer availability at the leading edge, $a(0)$, to polymerization flux, J_p, leads to our key result, the dependence of the rate of protrusion on biochemical parameters and resistance to motion. Indeed, recalling that the free polymerization velocity is $V_0 = k_{on}\delta a(0)$, and that the protrusion velocity is $V = V_0\exp(-w/B)$ by the force-velocity relation, we get

$$a(0) = Ve^{w/B}/k_{on}\delta.$$

Using expression (6) for the polymerization flux

$$J_p = BV/\delta\eta,$$

substituting the expressions for $a(0)$ and J_p into (23) and solving the resulting linear algebraic equation for V leads to the form of the protrusion velocity:

$$V = \frac{\bar{V}}{\kappa\exp(w/B) + \alpha B}, \qquad (25)$$

where

$$\bar{V} = k_{on}\delta A, \quad \kappa = \left(1 + \frac{k_3}{k_{-3}}\right), \quad \alpha = \left(\frac{k_{on}\tau}{\eta L}\right), \quad B = \frac{n}{\gamma}. \qquad (26)$$

The algebraic equation (25) expressing the protrusion velocity, V, as a function of the edge-density of leading barbed ends, B, is the main output of the model. We will be interested in what this equations implies about cell motion. A detailed interpretation of its form, and of the parameters in (26), is given in the following section. Subsequently, we draw conclusions about the way that the intricate machinery of the cell regulates rapid locomotion.

RESULTS

G-actin distribution

The model predicts stationary spatial distribution of sequestered G-actin complexes shown in Fig. 4 (see also Fig. 7). The concentrations of ADP-G-actin are constant and small over the lamellipod. Concentrations of ATP-G-actin complexes with profilin and thymosin are similar. They decrease from the rear to the front of the lamellipod over a range of 20–12 μM. This concentration gradient drives a flux of actin monomers toward the leading edge, feeding the extension of actin filament barbed ends. A result of the model is the estimate that the concentration of ATP-G-actin complexes with profilin at the leading edge available for polymerization is 13.75 μM. The total concentration of actin in various forms in the lamellipod is 1) F-actin, 210 μM; 2) total G-actin complexes, 40 μM. These results correspond to a realistic estimate of the depolymerization flux $J_d \sim J = 7\ \mu M\ s^{-1}$ and polymerization flux $J_p = 70\ \mu M \cdot \mu m\ s^{-1}$. The corresponding density of leading barbed ends is $85/\mu m$, which implies a protrusion velocity of $0.2\ \mu m\ s^{-1}$ according to the model.

Interpretation of the protrusion velocity

Three parameters, $\bar{V}$, κ, and α appear in expression 25 for the protrusion velocity. The numerator of this expression, $\bar{V} = k_{on}\delta A$, represents a hypothetical treadmilling velocity (in the absence of external load force) of a single actin filament fueled by a monomer pool equivalent to the total lamellipodial actin. (This is not an actual velocity in vivo, where many filaments compete for a much smaller monomer pool.) The first term in the denominator, $\kappa\exp(w/B)$, is the product of two dimensionless factors diminishing the rate of protrusion. From Fig. 3 and the definitions of k_3, k_{-3} we note that the ratio k_3/k_{-3} would represent approximately the ratio of the thymosin β4 to profilin forms of G-actin. Thus, the parameter $\kappa = 1 + (k_3/k_{-3})$ is a partition coefficient that captures the relative monomer availability. Its

presence in expression 25 effectively reduces the actin concentration, A, in the hypothetical treadmilling rate mentioned above.

The Boltzmann factor, $\exp(w/B)$, in Eq. 25 accounts for the effect of membrane resistance on damping the velocity. The second term in the denominator, αB, represents a drop in the velocity due to monomer pool depletion by competing barbed ends. Indeed, the number of uncapped barbed ends per unit area in the lamellipod is $\sim B/L$. The ratio k_{on}/η represents the rate of monomer assembly per end, and hence $k_{ass} = k_{on}B/\eta L$ [1 s^{-1}] corresponds roughly to the rate that monomers are assembling in total, over all barbed ends in the lamellipod. The parameter $1/\tau$ is an effective rate of delivery of actin from polymerized to the polymerization-competent monomer form. When B is large, and most of actin is in the polymerized form, the rate of assembly of actin has to balance the rate of delivery of the monomers, so that $k_{ass}a(0) \simeq A/\tau$. Thus, $a(0) \simeq A/(k_{ass}\tau)$. We see that the dimensionless factor $(k_{ass}\tau) = \alpha B$ represents the depletion of the actin pool due to polymerization. We will refer to α as the monomer depletion coefficient.

To understand what expression 25 implies, it is informative to consider two limiting cases. First consider the case that the number of leading barbed ends, B, is very small. Then the exponent in the Boltzmann factor $\exp(w/B)$ is large, while the depletion term αB is small. In this case, the first term in the denominator of V in (25) dominates, and

$$V \simeq \frac{\bar{V}}{\kappa \exp(w/B)}.$$

Most of the actin is then in monomer form, partitioned between profilin and thymosin, with the latter unavailable for polymerization, so A/κ is the concentration of G-actin available for polymerization, and $V \simeq k_{on}\delta(A/\kappa)\exp(-w/B)$ (a formula obtained from the polymerization ratchet model). The force generated by each filament, rather than monomer availability, limits the rate of protrusion. Protrusion decelerates exponentially as the load per filament increases. Thus, the velocity decreases sharply when the edge density of leading barbed ends decreases.

Now consider the opposite limiting case. If the number of leading barbed ends, B, is very large, the second term in the denominator of (25) dominates: $(w/B) \to 0$, $\exp(w/B) \to 1$, $\alpha B \gg \kappa \exp(w/B)$. In this case

$$V \simeq \frac{\bar{V}}{\alpha B}.$$

The actin monomer pool at the front is depleted and monomer availability, rather than membrane resistance, limits motility. In this case, the velocity decreases gradually and it becomes inversely proportional to B, as the density of the leading barbed ends increases.

Note that Carlier and Pantaloni (1997) predicted the same inverse relationship of the velocity on the number of the uncapped barbed ends. (See formula (6) in their paper under the assumption that there is no actin assembly at minus ends.) Thus, the funneling model (Carlier and Pantaloni, 1997) is, in a certain sense, a limiting case of our theory. Our model advances the original funneling hypothesis by including, and treating numerically, the effects of G-actin diffusion, sequestering, and membrane resistance. Note also that the predicted effect of the diffusion is small, as can be seen from Fig. 4. Effectively, diffusion causes a slight increase in the actin monomer turnover time τ, slowing protrusion. However, as noted before, the magnitude of the effect could be greater for a different set of model parameters than we have considered.

Protrusion is maximal at the optimal barbed end density

The total concentration of lamellipodial actin is estimated to be 100–1000 μM, and we use the value $A = 250$ μM. At this concentration the value of the treadmilling velocity is roughly $\bar{V} \simeq 5$ μm s^{-1}. For values of the model parameters used in this paper (Tables 1 and 2), $\kappa = 2$ and $\alpha \simeq 0.3$ μm. The protrusion velocity is shown as a function of the density of leading barbed ends in Fig. 6 for these parameter values and for characteristic values of the membrane resistance. This figure implies that *there is an optimal number of barbed ends for rapid cell motion*. We will refer to the value of this optimal barbed end density as B_o. The first limiting case discussed above corresponds to the suboptimal regime, $B < B_o$. It is significant that the velocity is particularly sensitive to the density B in this regime (note the sharp rise in the velocity up to its maximum here). The second limiting case corresponds to the regime in which $B > B_o$. Here, V changes much more gradually with B. At $B < B_o$ too few barbed ends cannot generate enough force to overcome the membrane resistance, while at $B > B_o$ too many barbed ends deplete the monomer pool and grow slowly. One implication of this result is that some sort of regulation of the barbed ends is needed: both the capping rate, γ, and the net nucleation rate, n, would have to be regulated so that the edge-density of leading barbed ends is close to optimal.

Estimating the maximal protrusion velocity and optimal barbed end density

The actual value of $B = B_o$, at which the protrusion velocity reaches its maximum, V_{max} (found using calculus and asymptotic analysis), is given in the Appendix. For physiological values of the model parameters (Tables 1 and 2), an approximation for the optimal density has a very simple form:

$$B_o \simeq w = \frac{F\delta}{k_B T}. \quad (27)$$

TABLE 2 Some dimensional values relevant to the model

Symbol	Value	Meaning	Reference
V	$\sim$0.25 μm sec^{-1}	Rate of protrusion	Abraham et al., 1999; Pollard et al., 2000; estimated in this paper
V_0	$k_{on}\delta a(0)$	Free polymerization velocity	Eq. 11
J_p	tens of μM $\cdot$ μm s^{-1}	Polymerization flux at the leading edge	Estimated in this paper
J	order of μM s^{-1}	Depolymerization flux	Estimated in this paper
B	$\sim$50–250 μm^{-1}	Density of barbed ends pushing membrane	Abraham et al., 1999; estimated in this paper
w	$\sim$50 μm^{-1}	Renormalized membrane resistance force per unit length	Estimated in this paper
H	$\simeq$0.17 μm	Thickness of the lamellipod	Abraham et al., 1999
P	$\sim$200 μM	Average concentration of actin in polymerized form	Estimated in this paper
τ	$\sim$30 s	Effective actin turnover time	Estimated in this paper
V	$\sim$5 μm s^{-1}	Hypothetical treadmilling rate	Estimated in this paper
α	$\sim$0.3 μm	Depletion coefficient	Estimated in this paper
κ	$\sim$2	Partition coefficient	Estimated in this paper
t_1	$\sim$30 s	Average time of uncapping of minus ends	Assumption
t_2, t_3	$\sim$1 s	Average time of complete disassembly of a filament with uncapped minus end	Estimated in this paper
k_s	$\sim$0.5 μm^{-1} s^{-1}	Rate of severing of a filament	Assumption
V_{dep}	$\sim$0.1 μm s^{-1}	Average disassembly rate of uncapped minus ends	Assumption, see also Carlier et al., 1999b

Thus, the model predicts that *the optimal number of uncapped barbed ends is proportional to the membrane resistance*. At a load force of $F \sim 100$ pN/μm, this value is $\sim B_o \sim 50/\mu$m. The observed density of barbed ends is on the order of $B \simeq 240$ per μm edge length (Abraham et al., 1999). It is likely that some of the observed barbed ends do not actually touch the membrane, so our estimate compares favorably with the experimental data.

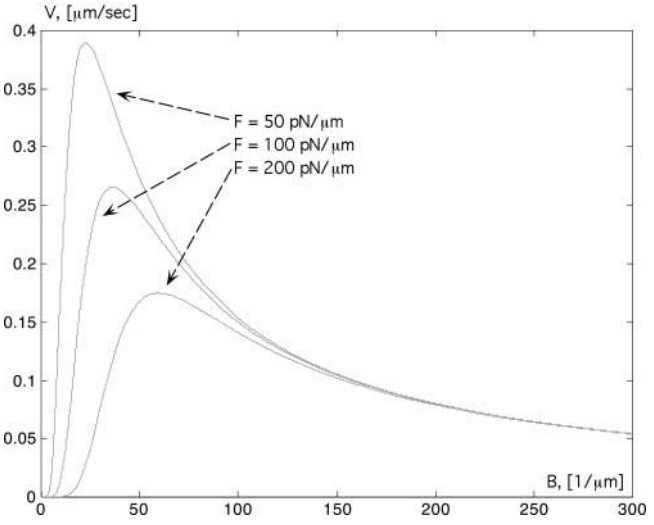

FIGURE 6 The protrusion velocity, V, is plotted as a function of the density of leading barbed ends, B, at three values of the membrane resistance. The velocity decreases dramatically when the density of the leading barbed ends drops below its optimal value. When the density of leading barbed ends is greater than optimal, the velocity decreases much more gradually. The maximal velocity is inversely proportional to the membrane resistance.

The corresponding maximal rate of protrusion, V_{max}, is found to be:

$$V_{max} \simeq \frac{\bar{V}}{e \cdot \kappa + \alpha \cdot w} \simeq 0.25\ \mu\text{m s}^{-1}.$$

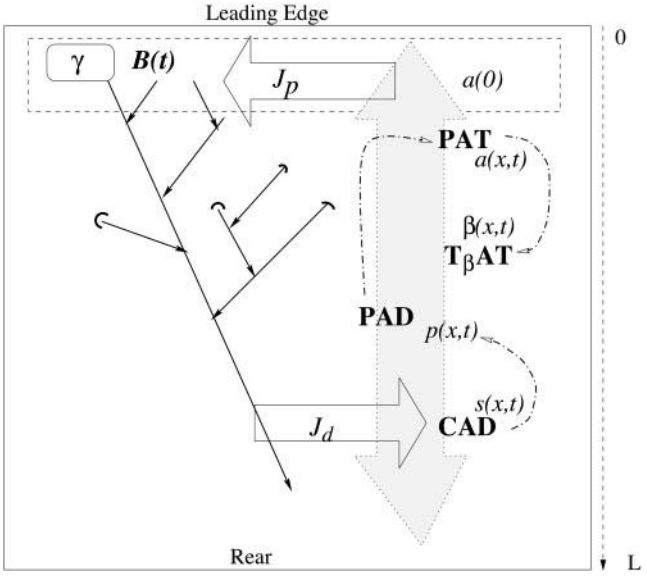

FIGURE 7 A schematic diagram showing the geometry assumed (1 dimension, $x = 0$ at leading edge, and x increasing toward the rear) and the interactions, sources, and sinks of the intermediates represented in the model: profilin-ADP-actin (PAD), cofilin-ADP-actin (CAD), profilin-ATP-actin (PAT), thymosin β4-ATP-actin (T_βAT), and actin filament barbed ends. *Clear arrows*: flux of polymerization and depolymerization. *Shaded arrow*: drift/diffusion of the G-actin complexes. *Dotted arrows*: exchange between G-actin monomer pools (see Fig. 3 for the rate constants). The polymerization flux is created by the leading barbed ends, $B(t)$. *Rounded rectangle*: rate of capping of barbed ends at the leading edge.

Note that this velocity is *proportional to the total amount of actin in the lamellipod* (recall $\bar{V}$ given in (26)). At the optimum, the *maximal velocity depends inversely on the membrane resistance*. The estimate is in good agreement with the experimentally observed range of locomotory rates (Pollard et al., 2000).

Protrusion depends weakly on thymosin β4

At physiological values of the model parameters (Tables 1 and 2), the maximal rate of protrusion $V_{\max}$ at $B = 50/\mu$m can be written in the form:

$$V_{\max} \simeq \frac{0.28\ \mu\text{m s}^{-1}}{1 + 0.15(T^*_\beta/T_\beta)},$$

where $T_\beta = 200\ \mu$M is the thymosin β4 concentration that we have used in our calculations, whereas T^*_β is some other possible value of this concentration. This formula demonstrates that if thymosin β4 concentration, T^*_β, were to increase 30-fold, from 20 to 600 μM (range cited in Pollard et al., 2000), then the velocity would decrease by much less than twofold, from 0.28 μm s^{-1} to 0.19 μm s^{-1}. Moreover, if the cell over-produces barbed ends, for example, if $B = 100/\mu$m, then

$$V \simeq \frac{0.17\ \mu\text{m s}^{-1}}{1 + 0.06(T^*_\beta/T_\beta)}.$$

(We will discuss this overproduction of barbed ends and its significance in terms of a regime of robust, resistance-independent locomotion in the next section.) In this case, if thymosin β4 concentration is increased from 20 to 600 μM, then the velocity decreases negligibly, from 0.17 μm s^{-1} to 0.15 μm s^{-1}. Thus, the model predicts that the protrusion velocity depends weakly on the thymosin β4 concentration in the physiological range, which is in agreement with observations (Boquet et al., 2000).

BIOLOGICAL IMPLICATIONS OF THE MODEL

The main result of this paper is that to achieve the maximal protrusion velocity, an optimal density of leading barbed ends is needed. At lower barbed end density, membrane resistance stalls forward growth. At higher density, the pool of actin monomers gets depleted too quickly, slowing polymerization in an "inverse funneling effect." Qualitatively, this conclusion is not surprising, and could be surmised without extensive mathematical modeling. However, our statements are quantitative, and lead to numerical estimates. Namely:

- Using available structural, biochemical, and mechanical data we have arrived at the estimate of *hundreds of nanometers per second as the order of magnitude of the protrusion velocity in rapidly moving cells*. This is in agreement with observed rates;
- The model predicts that *the optimal density of barbed ends is roughly proportional to membrane resistance*. At estimated values of the resistance, $F \sim 50$–500 pN/μm, we predict that the optimal density of barbed ends would be $B_o \sim 25$–$250/\mu$m. The observed value of $B \simeq 240/\mu$m (Abraham et al., 1999) probably includes barbed ends that are close to, but not actually pushing on, the cell membrane. Thus, the orders of magnitude of the theoretical estimate and the experimentally observed density match;
- The model predicts that *protrusion velocity is inversely proportional to the resistance force*. This prediction remains to be tested, but preliminary results (Raucher and Sheetz, 1999) are in agreement. A second prediction is that protrusion drops precipitously when the barbed end density is below a threshold proportional to the membrane tension. Furthermore, the protrusion rate decreases much more gradually as barbed end density increases above its optimal value;
- The model predicts that the *rate of steady motion is nearly independent of the thymosin β4 concentration* in the physiological range. This result is in agreement with observations (Boquet et al., 2000).
- The treadmilling model for the depolymerization pathway was here analyzed in a simplified quantitative setting. It predicts that the distribution of ADP-G-actin source disassembling from minus ends of actin filaments has a maximum close to the front of the cell. However, due to diffusion, the ADP-G-actin-profilin distribution is nearly homogeneous. Based on the quantitative analysis, we conclude that the model supports the funneling hypothesis (Dufort and Lumsden, 1996; Carlier et al., 1999b): we estimate that the number of uncapped minus ends across the lamellipod is an order of magnitude greater than the number of uncapped plus ends at the leading edge.

Based on the model results, we can speculate that the cell regulates the transition from stationary to motile state as well as the direction of motion (e.g., in chemotaxis) by rapidly and locally increasing the density of the uncapped barbed ends (for example, by activating more Arp2/3, or by locally cutting and uncapping filaments, or both), and/or locally decreasing membrane resistance by disrupting the adhesion of the cell cortex to the membrane. Our analysis shows that a modest (fewfold) change in the density of barbed ends and membrane resistance can change protrusion velocity dramatically. Indeed, the curves in Fig. 6 demonstrate that when the density of barbed ends changes from 25 to 50 per micron, and the membrane resistance simultaneously changes from 200 to 100 pN/μm, then the rate of protrusion increases from 25 nm s^{-1} to 250 nm s^{-1}.

Another attractive, though speculative, idea is that the cell could keep the density of barbed ends a few times higher than optimal to achieve *robust protrusion*. Indeed, Fig. 6 demonstrates this idea: suppose that the density of the barbed ends is 250/μm, as observed by Abraham et al., 1999. Then the protrusion of the cell is slower than optimal. However, in this range, protrusion no longer depends on membrane resistance (in the physiological range). The reason is that when the barbed ends are overproduced, the protrusion rate is limited by the availability of the ATP-G-actin, and not by mechanical resistance.

The number of actin barbed ends at the leading edge is regulated by the rates of nucleation and capping. Thus, the existence of an optimum barbed end density implies that there are optimal combinations of nucleation and capping rates. This prediction is in agreement with experimental results of Loisel et al. (1999) who observed a bell-shaped dependence of the motility rate of *Listeria* on the concentrations of Arp2/3 complexes and capping proteins.

Finally, one prediction worth noting is actually a corollary of the qualitative model: a greater amount of total actin and a faster rate of actin turnover correlate positively with the rate of locomotion. This latter result has been observed experimentally by McGrath et al. (2000) and by Loisel et al. (1999) who showed that there is an optimum in the concentration of ADF/cofilin for enhancing the rate of depolymerization.

Biological data needed to validate the model

Before the validity of the model can be conclusively assessed, further investigation of the actin nucleation pathways in the lamellipod, and particularly at the leading edge, is needed. A number of important questions must be resolved to distinguish between competing hypotheses, or modify existing assumptions we have made.

What are the true details of the actin depolymerization cycle? What relative roles do ADF/cofilin and gelsolin play? Is severing a significant part of the process or not? Severing could potentially enhance actin turnover while transiently generating many barbed ends across the lamellipod. Unless capped rapidly, these could deplete the actin monomer pool.

What is the spatial and temporal regulation of Arp2/3 complex activation and actin branching at the leading edge? How is capping of barbed ends regulated spatially at the leading edge? In particular, are the concentration of nucleating and capping agents limiting factors? If so, then reaction-diffusion equations for Arp2/3 and capping proteins would have to be introduced and incorporated into the model. One of the goals of this type of model could be to determine whether diffusion is sufficiently rapid to deliver these proteins to the leading edge. (It is not entirely clear that this is the case.) In case diffusion is insufficient, advection terms modeling protein delivery mediated by molecular motors (such as myosin I) could be investigated.

What is the corresponding effective rate of capping, γ? Indirectly, this rate could be estimated from data on the average length, l, of actin filaments: a simple kinematic argument suggests that $l \sim V/\gamma$, and $\gamma \sim V/l$. Unfortunately, such data are still controversial, but see Redmond and Zigmond (1993). Answering these questions will allow us to make assumptions that are more biologically precise, make predictions that are more accurate, and refine and/or possibly reject the model.

Experimental ways of testing the model

A number of experimental tests of the validity of our model are feasible, given statistics of measured keratocyte velocity. Phase contrast and/or electron microscopy can be used to estimate the density of membrane-associated ("leading") barbed ends: statistics for this density in relation to cell velocity can be compared to our Fig. 6. (Similarly, one could relate total lamellipodial actin to statistics on velocity and compare to predictions.) Careful measurements of G-actin density (Cramer, 1999; Svitkina and Borisy, 1999) as a function of the distance from the leading edge into the cell can be compared to our Figs. 5 and 6. One can envision controlled loading of a lamellipod with actin-sequestering agents such as thymosin to test how this impacts on cell velocity (Roy et al., 2001). Our model predicts no effect until the concentration of thymosin reaches the nM range, then a decrease in cell velocity as the thymosin level is increased. Similar experiments with controlled Arp2/3 and capping protein levels in vivo (e.g., as in Loisel et al., 1999; Laurent et al., 1999 in vitro) can be compared to our predicted bell-shaped velocity dependence. Coincidentally, our model predicts that in the presence of profilin, the steady-state concentration of ATP-G-actin is very small (as pointed out by an anonymous referee of this paper, this conclusion of the mathematical model has already been established experimentally (Pantaloni and Carlier, 1993)).

Limitations of the model

In constructing the model, we have made a large number of simplifications. Some of these are likely to limit the range of validity of the results. First, the boundary conditions at the rear edge of the lamellipod are not known and likely to be different from a no-flux condition. Second, the contractile stress in the lamellipod and the dynamic, graded adhesion of the cytoskeleton to the surface could affect the rate of protrusion. Third, the actual lamellipodial geometry is minimally two-dimensional, though we have reduced the model to a single space dimension. The sides of the lamellipod have very different dynamics from the front, and it is not clear whether or how they affect the protrusion process.

TABLE 3 Auxiliary rates and concentrations

Symbol	Value	Meaning	Note
P_r	10 μM	Total profilin conc.	5–100 μM physiological range (Pollard et al., 2000)
T_β	200 μM	Total thymosin β4 conc.	20–600 μM physiological range (Pollard et al., 2000)
S	10 μM	Total ADF/cofilin conc.	~20 μM physiological range (Pollard et al., 2000)
k_-^t	2.5 s^{-1}	T_βAT dissociation rate	Pollard et al., 2000; Dufort and Lumsden, 1996
k_+^t	1 μM^{-1} s^{-1}	T_βAT association rate	Pollard et al., 2000; Dufort and Lumsden, 1996
k_-^{pt}	5 s^{-1}	PAT dissociation rate	Pollard et al., 2000; Dufort and Lumsden, 1996
k_+^{pt}	50 μM^{-1} s^{-1}	PAT association rate	Pollard et al., 2000; Dufort and Lumsden, 1996
k_-^{pd}	10 s^{-1}	PAD dissociation rate	Rough estimate; Dufort and Lumsden, 1996
k_+^{pd}	15 μM^{-1} s^{-1}	PAD association rate	Rough estimate; Dufort and Lumsden, 1996
k_-^c	20 s^{-1}	CAD dissociation rate	Rough estimate; Pollard et al., 2000; Ressad et al., 1998
k_+^c	150 μM^{-1} s^{-1}	CAD association rate	Rough estimate; Pollard et al., 2000; Ressad et al., 1998

Dynamic lateral correlations along the leading edge can be very important. Fourth, the actual detailed force-velocity relation and dynamics of actin cortex responsible for the membrane resistance remains to be determined. Also, a large number of accessory proteins, not merely those few essential ones considered in the model, regulate protrusion. Finally, the process of protrusion can be pulsatile and non-stationary. These effects have not been considered in our model.

Is our model relevant only for the case of keratocyte cells? We would argue that other specialized cells have very similar properties. Nematode sperm cells, though devoid of actin, use an identical cytoskeletal mechanism: growth of a network at the front edge, disassembly at the rear, and firm adhesion in the middle (Roberts and Stewart, 2000; Bottino et al., 2002). In the more complex cells such as fibroblasts, leukocytes, and *Dictyostelium*, similar machinery may be at work, though the confounding influences of protrusion and retraction processes make these cases far more difficult to analyze. Even in such cases, we would argue that the model developed here has an important role to play: to make progress in this important field, whether via experiment or theory, we will be faced with the necessity of dissecting a complex and challenging set of phenomena into a simpler set of interacting components. These effects could then be more easily understood in isolation, making the problem of their full interactions more tractable in the long run.

Specifically in connection with the assumed geometry, we hope in the future to explore the dynamic (rather than steady-state) behavior of a 2-D extension of our model. This would help to address the dynamic nature of locomotion and would hopefully shed some light on chemotaxis. Such an extension of the model should allow us to quantitatively explain experiments in which inhibiting depolymerization leads to arrest of migration (Cramer, 1999).

Future efforts are needed to overcome all the above limitations of the model. This work is but an initial attempt to quantify one attractive hypothesis for the spatial and temporal regulation of locomotion of rapidly moving cells.

APPENDIX

Estimates of the model parameters

Diffusion coefficients

The cytoplasm has a high concentration of macromolecules, and this affects the rates of diffusion of substances such as actin monomers. We use the value $D \simeq 30\ \mu m^2\ s^{-1}$ (Abraham et al., 1999; Pollard et al., 2000). The sequestering agents profilin, thymosin, etc., considered here are small relative to an actin monomer (Bray, 1992) and their complexes with actin have a diffusion coefficient of a similar order of magnitude to that of free G-actin. We use the value $D = 30\ \mu m^2\ s^{-1}$ for the effective diffusion coefficients of G-actin complexes with the sequestering proteins.

Drift versus diffusion of small molecules

Here, we justify the omission of drift terms in our analysis of the actin monomer distribution in the lamellipod. The relative magnitudes of the diffusion and drift terms in Eqs. 2–5 is given by a dimensionless factor (D/lV), where l is a spatial scale. One of the natural spatial scales in the model is the lamellipodial length $L \sim 10\ \mu m$. The corresponding characteristic value of the dimensionless factor is $(D/LV) \sim (30\ \mu m^2\ s^{-1})/(10\ \mu m \cdot 0.3\ \mu m\ s^{-1}) = 10$. The contrast between diffusion and drift is even greater on any relevant spatial scale smaller than the lamellipodial length. Thus, it is reasonable to neglect the first-order spatial derivative terms in Eqs. 2–5.

Derivation of the conversion factor η

The factor η [$\mu M^{-1}\ \mu m^{-2}$] converts μM concentration units into the number of molecules per unit area of the lamellipod, given that the lamellipod thickness is $\simeq 0.17\ \mu m$ (Abraham et al., 1999). A concentration of 1 μM corresponds to $\simeq 600$ molecules/μm^3 and this corresponds to $0.17 \cdot 600 \simeq 100$ molecules per 1 μm^2 of the lamellipod. Thus, $\eta \simeq 100\ \mu M^{-1}\ \mu m^{-2}$.

Reaction rates

Order of magnitude estimates of the reaction rates are based on known rates of G-actin association and dissociation with ADF/cofilin, profilin, and thymosin β4, nucleotide exchange, and concentrations of the sequestering proteins. We use values (Table 3) cited in Dufort and Lumsden, 1996; Pollard et al., 2000; and Ressad et al., 1998 where original citations of the relevant experimental papers can be found. Because underlying biochemical data stems from a variety of cell types and experimental conditions, these values should be interpreted as ball-park figures.

Under physiological conditions there is ~200 μM of ATP and ~20 μM of ADP in the cell. The rate-limiting step in ADP-ATP exchange on profilin-ADP-actin under these conditions is the dissociation of ADP, with rate constant $k_2 \sim 20\ s^{-1}$.

Concentrations and rates of reactions among actin monomers, profilin-ATP-actin, and thymosin-ATP-actin are shown in Table 3. The effective rates of ATP-G-actin association with profilin and thymosin are then $\bar{k}_+^{pt} = k_+^{pt}P = 500\ s^{-1}$ and $\bar{k}_+^{t} = k_+^{t}T_\beta = 200\ s^{-1}$, much faster than the dissociation rates of the corresponding complexes. This implies that the concentration of free ATP-G-actin is very small relative to sequestered ATP-G-actin. Furthermore, free ATP-G-actin rapidly approaches its equilibrium concentration, g_t, obtained from equating association and dissociation rates:

$$(\bar{k}_+^{pt} + \bar{k}_+^{t})g_t = k_-^{pt}a + k_-^{t}\beta, \quad g_t = \frac{k_-^{pt}a + k_-^{t}\beta}{\bar{k}_+^{pt} + \bar{k}_+^{t}}.$$

The equations for the dynamics of sequestered ATP-G-actin:

$$\frac{da}{dt} = -k_-^{pt}a + \bar{k}_+^{pt}g_t,$$

$$\frac{d\beta}{dt} = -k_-^{t}\beta + \bar{k}_+^{t}g_t,$$

can then be rewritten in the form:

$$\frac{da}{dt} = -\frac{d\beta}{dt} = -k_3 a + k_{-3}\beta,$$

where

$$k_{-3} = k_-^{pt}\frac{\bar{k}_+^{pt}}{\bar{k}_+^{pt} + \bar{k}_+^{t}} \simeq 2/\text{sec},$$

$$k_3 = k_-^{t}\frac{\bar{k}_+^{t}}{\bar{k}_+^{pt} + \bar{k}_+^{t}} \simeq 2/\text{sec}.$$

For the reactions between ADP-G-actin with profilin or ADF/cofilin (see also Table 3) we have effective rates of association $\bar{k}_+^{pd} = k_+^{pd}P_r = 150\ s^{-1}$ and $\bar{k}_+^{s} = k_+^{s}S = 1500\ s^{-1}$, respectively, again much faster than the dissociation rates of the corresponding complexes. As in the case of profilin/thymosin above, the concentration of free ADP-G-actin rapidly approaches a low equilibrium level, g_d, obtained from

$$(\bar{k}_+^{pd} + \bar{k}_+^{s})g_d = k_-^{pd}p + k_-^{s}s, \quad g_d = \frac{k_-^{pd}p + k_-^{s}s}{\bar{k}_+^{pd} + \bar{k}_+^{s}}.$$

The equations for sequestered ADP-G-actin:

$$\frac{dp}{dt} = -k_-^{pd}p + \bar{k}_+^{pd}g_d, \quad \frac{ds}{dt} = -k_-^{s}s + \bar{k}_+^{s}g_d,$$

can also be rewritten in the form:

$$\frac{dp}{dt} = -\frac{ds}{dt} = -k_{-1}p + k_1 s,$$

where

$$k_1 = k_-^{s}\frac{\bar{k}_+^{pd}}{\bar{k}_+^{pd} + \bar{k}_+^{s}} \simeq 2/\text{s},$$

$$k_{-1} = k_-^{pd}\frac{\bar{k}_+^{s}}{\bar{k}_+^{pd} + \bar{k}_+^{s}} \simeq 10/\text{s}.$$

This analysis demonstrates that almost all G-actin in the lamellipod is sequestered, and that the concentration of free G-actin is negligible.

Solution of equations of the treadmilling model and discussion of tread-severing model

Equations 7–9 can be nondimensionalized by choosing $m_c(0)$ as the scale of the density of the capped minus ends, $m_c(0)(t_2/t_1)$, as the scale of the density of the uncapped minus ends; t_2V as the length scale; and t_2 as the time scale. The corresponding stationary solutions are governed by the system of ODEs:

$$\frac{dm_c'}{dx'} = -\epsilon m_c', \quad \frac{dm'}{dx'} = m_c' - m',$$

$$m_c'(0) = 1, \quad m'(0) = 0, \quad \epsilon = t_2/t_1 \ll 1,$$

where primes denote the dimensionless variables. The solutions of these equations are:

$$m_c'(x') = e^{-\epsilon x'},\ m'(x') = (e^{-\epsilon x'} - e^{-x'}).$$

Corresponding dimensional expressions are given by the formulae (18, 19).

In the alternative hypothesis for depolymerization, the tread-severing model, the distal ends of growing actin filaments are severed by ADF/cofilin, by gelsolin, or by a combination of both, leading to breaks in the filaments and new ends. Any resulting new minus ends, so created, depolymerize, producing a source of G-actin. Incorporating this scenario for depolymerization in our model requires that we consider the actin filament density. Let $f(x, t)$ denote the length density of F-actin (e.g., in units of μm filament length per μm^2 lamellipodial area, or simply number of filaments intersecting a 1 μm transect.) At the leading edge, this density can be approximated by the edge density of the barbed ends, $B(t)$, since each filament traversing a little edge square has a barbed end at its head.

Let k_s [$\mu m^{-1}\ s^{-1}$] denote the rate of severing of a filament, assumed constant: i.e., a filament of length l gets severed on average every $1/(k_s l)$ s. We will assume that severing is limited by a slow process so that $1/(k_s l)$ is relatively large compared to the depolymerization time. Severing creates two new filaments of average length $l/2$. At the site of the break, this forms one new uncapped minus end that starts to depolymerize.

The time taken for disassembly of the cut filament at its new minus end is on the order of $t_3 \sim l/2V_{dep} \sim 1$ s. Our assumption about the slow rate of severing is taken to mean that $1/(k_s l) \gg t_3$, and implies that a new filament usually disassembles completely before it can be cut once more. In the model, we use the value $1/(k_s l) = 30$ s, $k_s \sim 0.5\ \mu m^{-1}\ s^{-1}$.

Given the assumptions and simplifications described here, the dynamics of filament density in the tread-severing scenario are described by the system of equations:

$$\frac{\partial f}{\partial t} = -V\frac{\partial f}{\partial x} - V_{dep}m, \tag{28}$$

$$\frac{\partial m}{\partial t} = -V\frac{\partial m}{\partial x} + k_s f - \frac{m}{t_3}, \tag{29}$$

$$f(0) = B, \quad m(0) = 0. \tag{30}$$

The term $-V_{dep}m$ in Eq. 28 accounts for loss of F-actin due to depolymerization at the uncapped minus ends. As in the array treadmilling version, we here neglect effective movement of uncapped minus ends toward the front, because the depolymerization velocity is much slower than the protrusion velocity.

Equations 28–30 can be nondimensionalized by choosing $f(0)$ as the scale of the length density of F-actin, $f(0)t_3k_s$ as the scale of the density of

the uncapped minus ends, t_3V as the length scale, and t_3 as the time scale. The corresponding stationary solutions are governed by the system of ODEs:

$$\frac{df'}{dx'} = -\epsilon m', \quad \frac{dm'}{dx'} = f' - m', \quad f'(0) = 1,$$

$$m'(0) = 0, \quad \epsilon = V_{dep}k_s(t_3)^2 \ll 1,$$

where primes denote dimensionless variables. The solutions of these equations are:

$$m'(x') = A(e^{-\rho_1 x'} - e^{-\rho_2 x'}),$$

$$f'(x') = A(e^{-\rho_1 x'} - e^{-\rho_2 x'} - \rho_1 e^{-\rho_1 x'} + \rho_2 e^{-\rho_2 x'}),$$

where $\rho_{1,2} = \frac{1}{2}(1 \mp \sqrt{1 - 4\epsilon})$. These expressions can be simplified by using the fact that $\rho_1 \simeq \epsilon$ and $\rho_2 \simeq 1$. Then, $A \simeq 1$ and the nondimensional solutions of the tread-severing model become:

$$m'(x') \simeq (e^{-\epsilon x'} - e^{-x'}), \quad f'(x') \simeq e^{-\epsilon x'}.$$

Corresponding dimensional expressions are:

$$f(x) \simeq \frac{n}{\gamma} \exp\left(-\frac{V_{dep}k_s t_3}{V} x\right), \tag{31}$$

$$m(x) \simeq \frac{n}{\gamma} k_s t_3 \left[\exp\left(-\frac{V_{dep}k_s t_3}{V} x\right) - \exp\left(-\frac{1}{Vt_3} x\right)\right] \tag{32}$$

Both tread-severing and treadmilling models predict identical expressions for the density of uncapped pointed ends and the distribution of the G-actin source (however, the meanings of the parameters governing the processes are distinct). Nevertheless, we only described the tread-severing model of depolymerization in the Appendix, rather than in the body of the paper, because this model implies "side effects" that hinder rapid lamellipodial protrusion. First, the value of the severing rate $k_s \sim 0.5\ \mu m^{-1}\ s^{-1}$ that is necessary to maintain fast actin turnover is hard to reconcile with much smaller rate suggested indirectly by experiments (Ressad et al., 1999). More importantly, in the process of severing, barbed ends are created simultaneously with minus ends. These barbed ends would grow, depleting the ATP-G-actin pool. It could be argued that these are rapidly capped to avoid the depletion. Here we consider this problem quantitatively.

We argue above that when the number of leading barbed ends, B, is large, and the membrane resistance does not limit the actin turnover, then the concentration of ATP-G-actin at the leading edge, $a(0) \simeq A/(k_{ass}\tau)$, where $k_{ass} = k_{on}B/(\eta L)$ is the rate of monomer assembly. This result was obtained under the assumption that all uncapped barbed ends are at the front of the lamellipod. Order of magnitude estimates give the following simple and intuitively clear result: if b_1 uncapped barbed ends are distributed across the lamellipodial length, in addition to B leading barbed ends, then the rate of monomer assembly is proportional to the total number of the uncapped barbed ends, $k_{ass} = k_{on}(B + b_1)/(\eta L)$. Thus, $a(0) \sim (B + b_1)^{-1}$. Barbed ends are created in the process of severing at the same rate as minus ends, so the number of barbed ends distributed across the lamellipod is equal to the total number of uncapped minus ends times the ratio of the rates of disappearance of the minus ends to the rate of capping of the barbed ends. Above we estimated the number of the uncapped minus ends to be an order of magnitude greater than the number of leading barbed ends. Thus, for the number of other uncapped barbed ends to be of the same order as that of the leading barbed ends (or less), the rate of capping in the lamellipod has to be $\sim$10/s or faster. Reported capping rates by known capping proteins are slower, $\sim$1/s. It is unclear if gelsolin caps the barbed ends fast enough; some observations suggest that the corresponding capping rates are slow (Gremm and Wegner, 2000). If the effective capping rate is $\sim$1/s, then $b_1 \simeq 10 \cdot B$, and the growing barbed ends created by severing would decrease $a(0)$, and the rate of the protrusion by an order of magnitude.

In the other limiting case, when the number of leading barbed ends is small, and the membrane resistance is rate-limiting, the situation is even worse, because the growth of the leading barbed ends is slower, while that of the other ends is free and fast. Finally, there could be a problem of lamellipodial swelling due to this growth across the lamellipod. Further observations and measurements of the capping rates are needed to either alter or reject the tread-severing model.

Sequestered ATP-G-actin

We consider the equations

$$D\frac{d^2\beta}{dx^2} - k_{-3}\beta + k_3 a = 0,$$

$$D\frac{d^2a}{dx^2} + k_{-3}\beta - k_3 a + J = 0,$$

for profilin- and thymosin-actin, together with the boundary conditions:

$$\frac{da}{dx}(0) = J_p/D, \quad \frac{da}{dx}(L) = \frac{d\beta}{dx}(0) = \frac{d\beta}{dx}(0) = 0.$$

We first observe that by adding the two differential equations, and integrating over x we get:

$$\frac{d}{dx}(\beta + a) = -\frac{Jx}{D} + \frac{J_p}{D},$$

(where we have used two boundary conditions). Furthermore, continuing the integration leads to

$$\beta(x) + a(x) = -\frac{Jx^2}{2D} + \frac{J_p x}{D} + C,$$

for some constant C. This connection can be used to eliminate one of the variables from either of the original ODEs. For example, we can express the first equation in the form

$$D\frac{d^2\beta}{dx^2} - (k_{-3} + k_3)\beta = f(x),$$

where $f(x)$ is a known expression involving x. The solution to the system will thus involve exponentials with eigenvalues $\pm\sqrt{(k_{-3} + k_3)/D}$ superimposed on particular solutions. It can be checked by substitution that the resulting solutions have the form:

$$a(x) = \frac{c_1 + c_2 x}{k_3} + \frac{k_3 J}{(k_3 + k_{-3})^2} - \frac{k_{-3}Jx^2}{2D(k_3 + k_{-3})} + c_3 e^{\lambda x} - c_4 e^{-\lambda x}, \tag{33}$$

$$\beta(x) = \frac{c_1 + c_2 x}{k_{-3}} - \frac{k_3 J}{(k_3 + k_{-3})^2} - \frac{k_3 Jx^2}{2D(k_3 + k_{-3})} - c_3 e^{\lambda x} + c_4 e^{-\lambda x}, \tag{34}$$

where

$$\lambda = \sqrt{\frac{k_3 + k_{-3}}{D}} \equiv \frac{1}{L_a}. \quad (35)$$

Because we have two second-order equations, there are four arbitrary coefficients, c_i, $i = 1 \ldots 4$. These are determined from the four boundary conditions.

The boundary conditions at $x = 0$ lead to the equations:

$$\frac{c_2}{k_{-3}} - \lambda c_3 - \lambda c_4 = 0, \quad (36)$$

$$\frac{c_2}{k_3} + \lambda c_3 + \lambda c_4 = \frac{J_p}{D}. \quad (37)$$

The boundary conditions at $x = L$ yields:

$$\frac{c_2}{k_{-3}} - \frac{Jk_3L}{D(k_3 + k_{-3})} - \lambda c_3 e^{\lambda L} - \lambda c_4 e^{-\lambda L} = 0, \quad (38)$$

$$\frac{c_2}{k_3} - \frac{Jk_{-3}L}{D(k_3 + k_{-3})} + \lambda c_3 e^{\lambda L} + \lambda c_4 e^{-\lambda L} = 0. \quad (39)$$

Adding equations 36 and 37 leads to the expression for the coefficient c_2:

$$c_2 = \frac{k_3 k_{-3}}{k_3 + k_{-3}} \frac{J_p}{D}. \quad (40)$$

Substituting this expression for c_2 into equations 38 and 39 and adding the equations results in:

$$J_p = JL, \quad \text{or} \quad J = J_p/L.$$

This formula provides a restriction on the total fluxes of depolymerization, JL, and polymerization, J_p, (both in dimensions [μM (μm s^{-1})]): at steady motion with constant velocity, when the total amounts of G-actin and F-actin do not change with time, these fluxes must balance.

The coefficients c_3 and c_4 can be estimated if we first subtract (37) from (36), then (38) from (39), and use formula (40):

$$c_3 \simeq 0, \quad c_4 \simeq \frac{k_3}{k_3 + k_{-3}} \frac{J_p}{D\lambda}. \quad (41)$$

To obtain the approximation, we used the fact that $L \simeq 10$ μm, $L_a \simeq 2.5$ μm, and $\exp[-\lambda L] = \exp[-L/L_a] \simeq 0.04$. The neglected terms are exponentially small (i.e., of order $O(\exp[-\lambda L])$.

From our initial observations, as well as detailed solutions, we have expressions for $\beta(x) + a(x)$. Integrating over the length of the lamellipod ($0 < x < L$), using the expressions for the coefficients $c_{2,3,4}$ found above, and using the connection $J = J_p/L$, we find that the amount of sequestered ATP-G-actin is:

$$\bar{a} + \bar{\beta} \equiv \frac{1}{L} \int_0^L (a(x) + \beta(x)) dx$$

$$= c_1 \frac{k_3 + k_{-3}}{k_3 k_{-3}} + \frac{J_p L}{3D}. \quad (42)$$

The coefficient c_1, undetermined at this point, can be found from conservation of the total amount of actin in the lamellipod in all its forms, denoted by A [μM]. (A is actually total actin concentration.) We make the simplest possible assumption about depolymerization dynamics, i.e., that the depolymerization flux, J, is equal to rP, where r [1 s^{-1}] is the effective depolymerization rate, and P [μM] is the amount of actin in polymerized form. Using the condition $J_p = JL$, we estimate the amount of F-actin as $P = J_p/rL$. Consequently, the total amount of G-actin is $(\bar{a} + \bar{\beta} + s + p) = (A - J_p/rL)$.

Using Eq. 42 and expressions (22) for the amount of the ADP-G-actin, $s + p$, we find the coefficient c_1:

$$c_1 = \frac{k_3 k_{-3}}{k_3 + k_{-3}} \left(A - (\tau_{dep} + \tau_{cof} + \tau_{dif}) \frac{J_p}{L} \right). \quad (43)$$

Here

$$\tau_{cof} = \frac{k_1 + k_{-1} + k_2}{k_1 k_2}, \quad \tau_{dep} = \frac{1}{r}, \quad \tau_{dif} = \frac{L^2}{3D}. \quad (44)$$

Substituting this expression into Eq. 33 and evaluating it at $x = 0$, we find the concentration of polymerization-competent actin at the leading edge:

$$a(0) = \frac{k_{-3}}{k_3 + k_{-3}} \left(A - \frac{J_p \tau}{L} \right), \quad (45)$$

where

$$\tau = \tau_{dep} + \tau_{cof} + \tau_{dif} + \tau_{thy} \quad (46)$$

is the total monomer recycling time and

$$\tau_{thy} = \frac{k_3}{k_{-3}(k_3 + k_{-3})} \left[\sqrt{\frac{L^2(k_3 + k_{-3})}{D}} - 1 \right]. \quad (47)$$

is the mean lifetime of an actin-thymosin complex. Note that expression (47) for τ_{thy} is a valid approximation when the strong inequality $L \gg L_a = \sqrt{D/(k_3 + k_{-3})}$ is satisfied (recall that $L \simeq 10$ μm, $L_a \simeq 2.5$ μm). Formulae 45–47 justify Eqs. 23 and 24. The parameter τ_{rec} in Eq. 24 is defined as $\tau_{rec} = \tau_{dif} + \tau_{thy}$.

The optimal number of barbed ends

The optimal number of leading barbed ends corresponds to the value of B for which the denominator of (25) has a minimum. Differentiating the denominator, $(\kappa \exp[w/B] + \alpha B)$ with respect to B, we find that the minimum is achieved at $B = B_o$ satisfying $(w/B_o^2)\exp[w/B_o] = (\alpha/\kappa)$. In terms of the dimensionless variable $x = w/B$ and the parameter $\epsilon = \alpha w/\kappa$, we can rewrite this equation in the form: $\exp(x) = \epsilon/x^2$. For positive x, this equation has a unique solution that can be found numerically (e.g., using the bisection method). For parameter values $\kappa = 2$, $\alpha = 0.3$ μm^{-1}, $w = 50$ μm^{-1}, the numerical solution is $x \simeq 1$. When the membrane resistance changes by one order of magnitude, from 50 to 500 pN/μm, this solution changes only two-fold: $0.75 < x < 1.6$. Thus, a good order of magnitude estimate for the optimal number of leading barbed ends is: $x \simeq 1$, or $B_o \simeq w$.

We are grateful to G. Borisy and T. Pollard for fruitful discussions. We also thank anonymous reviewers for helpful suggestions and criticism.

A.M. is supported by a University of California-Davis Chancellor's Fellowship, National Science Foundation Grant DMS-1097746, and a National Institutes of Health Glue grant "Cell Migration Consortium." L.E.K. is supported by a Natural Sciences and Engineering Research Council (Canada) operating grant.

REFERENCES

Abraham, V. C., V. Krishnamurthi, D. L. Taylor, and F. Lanni. 1999. The actin-based nanomachine at the leading edge of migrating cells. *Biophys. J.* 77:1721–1732.

Amann, K. J., and T. D. Pollard. 2001. The Arp2/3 complex nucleates actin filament branches from the sides of pre-existing filaments. *Nat. Cell Biol.* 3:306–310.

Bailly, M., F. Macaluso, M. Cammer, A. Chan, J. E. Segall, and J. S. Condeelis. 1999. Relationship between Arp2/3 complex and the barbed ends of actin filaments at the leading edge of carcinoma cells after epidermal growth factor stimulation. *J. Cell Biol.* 145:331–345.

Beningo, K., M. Dembo, I. Kaverina, J. Small, and Y. Wang. 2001. Nascent focal adhesions are responsible for the generation of strong propulsive forces in migrating fibroblasts. *J. Cell Biol.* 153:881–888.

Blanchoin, L., K. J. Amann, H. N. Higgs, J. B. Marchand, D. A. Kaiser, and T. D. Pollard. 2000a. Direct observation of dendritic actin filament networks nucleated by Arp2/3 complex and WASP/Scar proteins. *Nature.* 404:1007–1011.

Blanchoin, L., T. D. Pollard, and S. E. Hitchkock-DeGregori. 2001. Inhibition of the Arp2/3 complex-nucleated actin polymerization and branch formation by tropomyosin. *Curr. Biol.* 11:1300–1304.

Boquet, I., R. Boujemaa, M. F. Carlier, and T. Prat. 2000. Ciboulot regulates actin assembly during Drosophila brain metamorphosis. *Cell.* 102:797–800.

Bottino, D., A. Mogilner, T. Roberts, M. Stewart, and G. Oster. 2002. How nematode sperm crawl. *J. Cell Sci.* 115:367–384.

Bray, D. 1992. Cell Movements. Garland, New York.

Cameron, L. A., P. A. Giardini, F. S. Soo, and J. A. Theriot. 2000. Secrets of actin-based motility revealed by a bacterial pathogen. *Nat. Rev. Mol. Cell Biol.* 1:110–119.

Carlier, M. F., A. Ducruix, and D. Pantaloni. 1999a. Signalling to actin: the Cdc42-N-WASP-Arp2/3 connection. *Chemistry and Biology* (*London*). 6:R235–R240.

Carlier, M. F., P. Nioche, I. Broutin-L'Hermite, R. Boujemaa, C. L. Clainche, C. Egile, C. Garbay, A. Ducruix, P. Sansonetti, and D. Pantaloni. 2000. GRB2 links signaling to actin assembly by enhancing interaction of Neural Wiskott-Aldrich Syndrome Protein (N-WASp) with actin-related protein (ARP2/3) complex. *J. Biol. Chem.* 275: 21946–21952.

Carlier, M. F., and D. Pantaloni. 1997. Control of actin dynamics in cell motility. *J. Mol. Biol.* 269:459–467.

Carlier, M. F., D. Pantaloni, and E. Korn. 1986. The effects of Mg^{2+} at the high affinity sites on the polymerization of actin and associated ATP hydrolysis. *J. Biol. Chem.* 261:10785–10792.

Carlier, M. F., F. Ressad, and D. Pantaloni. 1999b. Control of actin dynamics in cell motility. *J. Biol. Chem.* 274:33827–33830.

Chen, H., B. W. Bernstein, and J. R. Bamburg. 2000. Regulating actin-filament dynamics in vivo. *TIBS.* 25:19–23.

Coluccio, L. M., and L. G. Tilney. 1983. Under physiological conditions actin disassembles slowly from the nonpreferred end of an actin filament. *J. Cell Biol.* 97:1629–1634.

Cramer, L. P. 1999. Role of actin filament disassembly in lamellipodium protrusion in motile cells revealed using the drug jasplakinolide. *Curr. Biol.* 9:1095–1105.

Dai, J. W., and M. P. Sheetz. 1999. Membrane tether formation from blebbing cells. *Biophys. J.* 77:3363–3370.

Dai, J., M. P. Sheetz, X. Wan, and C. E. Morris. 1998. Membrane tension in swelling and shrinking molluscan neurons. *J. Neurosci.* 18: 6681–6692.

Dufort, P. A., and C. J. Lumsden. 1996. How profilin/barbed-end synergy controls actin polymerization: a kinetic model of the ATP hydrolysis circuit. *Cell Motil. Cytoskel.* 35:309–330.

Egile, C., T. P. Loisel, V. Laurent, R. Li, D. Pantaloni, P. J. Sansonetti, and M. F. Carlier. 1999. Activation of the CDC42 effector N-WASP by the *Shigella flexneri* IcsA protein promotes actin nucleation by Arp2/3 complex and bacterial actin-based motility. *J. Cell Biol.* 146:1319–1332.

Erickson, C. A. 1980. The deformability of BHK cells in relation to locomotory behavior. *J. Cell Sci.* 44:187–200.

Evans, E., and R. Skalak. 1980. Mechanics and Thermodynamics of Biomembranes. CRC Press, Boca Raton, FL.

Gerbal, F., P. Chaikin, Y. Rabbin, and J. Prost. 2000. Elastic model of *Listeria* propulsion. *Biophys. J.* 79:2259–2275.

Gerisch, G. 1982. Chemotaxis in *Dictyostelium*. *Annu. Rev. Physiol.* 44: 535–552.

Gremm, D., and A. Wegner. 2000. Gelsolin as a calcium-regulated actin filament-capping protein. *Eur. J. Biochem.* 267:4339–4345.

Hartwig, J. H., G. M. Bokoch, C. L. Carpenter, P. A. Janmey, L. A. Taylor, A. Toker, and T. P. Stossel. 1995. Thrombin receptor ligation and activated rac uncap actin filament barbed ends through phosphoinositide synthesis in permeabilized human platelets. *Cell.* 82:643–653.

Higgs, H. N., L. Blanchoin, and T. D. Pollard. 1999. Influence of the C terminus of Wiskott-Aldrich syndrome protein (WASp) of the Arp2/3 complex on actin polymerization. *Biochemistry.* 38:15212–15222.

Higgs, H. N., and T. D. Pollard. 1999. Regulation of actin polymerization by Arp2/3 complex and WASp/Scar proteins. *J. Biol. Chem.* 274: 32531–32534.

Hill, T. L. 1987. Linear Aggregation Theory in Cell Biology. Springer, New York.

Hill, T. L., and M. W. Kirschner. 1982. Bioenergetics and kinetics of microtubule and actin filament assembly-disassembly. *Int. Rev. Cytol.* 78:1–125.

Hochmuth, F. M., J. Y. Shao, J. Dai, and M. P. Sheetz. 1996. Deformation and flow of membrane into tethers extracted from neuronal growth cones. *Biophys. J.* 70:358–369.

Huang, M., C. Yang, D. A. Schafer, J. A. Cooper, H. N. Higgs, and S. H. Zigmond. 1999. Cdc42-induced actin filaments are protected from capping protein. *Curr. Biol.* 9:979–982.

Kelleher, J. F., S. J. Atkinson, and T. D. Pollard. 1995. Sequences, structural models, and cellular localization of the actin-related proteins Arp2 and Arp3 from *Acanthamoeba*. *J. Cell Biol.* 131:385–397.

Korn, E. D., M. F. Carlier, and D. Pantaloni. 1987. Actin filament polymerization and ATP hydrolysis. *Science.* 238:638–644.

Laurent, V., T. P. Loisel, B. Harbeck, A. Wehman, L. Grobe, B. M. Jockusch, J. Wehland, F. B. Gertler, and M. F. Carlier. 1999. Role of proteins of the Ena/VASP family in actin-based motility of *Listeria monocytogenes*. *J. Cell Biol.* 144:1245–1258.

Lee, J., and K. Jacobson. 1997. The composition and dynamics of cell-substratum adhesions in locomoting fish keratocytes. *J. Cell Sci.* 110: 2833–2844.

Loisel, T. P., R. Boujemaa, D. Pantaloni, and M. F. Carlier. 1999. Reconstitution of actin-based motility of *Listeria* and *Shigella* using pure proteins. *Nature.* 401:613–616.

Ma, L., R. Rohatgi, and M. W. Kirschner. 1998. The Apr2/3 complex mediates actin polymerization induced by the small GTP-binding protein Cdc42. *Proc. Natl. Acad. Sci. U.S.A.* 95:15362–15367.

Machesky, L. M. 1997. Cell motility: complex dynamics at the leading edge. *Curr. Biol.* 7:R164–R167.

Machesky, L. M., and R. H. Insall. 1999. Signaling to actin dynamics. *J. Cell Biol.* 146:267–272.

Machesky, L. M., R. D. Mullins, H. N. Higgs, D. A. Kaiser, L. Blanchoin, R. C. May, M. E. Hall, and T. D. Pollard. 1999. Scar, a WASp-related protein, activates nucleation of actin filaments by the Arp2/3 complex. *PNAS.* 96:3739–3744.

Maly, I. V., and G. G. Borisy. 2001. Self-organization of a propulsive actin network as an evolutionary process. *Proc. Natl. Acad. Sci. U.S.A.* 98: 11324–11329.

Marchand, J., P. Moreau, A. Paoletti, P. Cossart, M. F. Carlier, and D. Pantaloni. 1995. Actin-based movement of *Listeria monocytogenes*: actin assembly results from the local maintenance of uncapped filament barbed ends at the bacterium surface. *J. Cell Biol.* 130:331–343.

McGrath, J. L., E. A. Osborn, Y. S. Tardy, C. F. D., Jr., and J. H. Hartwig. 2000. Regulation of the actin cycle in vivo by actin filament severing. *PNAS.* 97:6532–6537.

Mitchison, T. J., and L. P. Cramer. 1996. Actin-based cell motility and cell locomotion. *Cell.* 84:371–379.

Mogilner, A., E. Marland, and D. Bottino. 2001. A minimal model of locomotion applied to the steady "gliding" movement of fish keratocyte cells. *In* Pattern Formation and Morphogenesis: Basic Processes. H. Othmer and P. Maini, editors. Springer-Verlag, New York. 269–294.

Mogilner, A., and G. Oster. 1996a. Cell motility driven by actin polymerization. *Biophys. J.* 71:3030–3045.

Mogilner, A., and G. Oster. 1999. The polymerization ratchet model explains the force-velocity relation for growing microtubules. *Eur. J. Biophys.* 28:235–242.

Mullins, R. D., J. A. Heuser, and T. D. Pollard. 1998. The interaction of Arp2/3 complex with actin: nucleation, high affinity pointed end capping, and formation of branching networks of filaments. *PNAS.* 95: 6181–6186.

Mullins, R. D., W. F. Stafford, and T. D. Pollard. 1997. Structure, subunit topology, and actin-binding activity of the Arp2/3 complex from Acanthamoeba. *J. Cell Biol.* 136:331–343.

Munevar, S., Y. Wang, and M. Dembo. 2001. Distinct roles of frontal and rear cell-substrate adhesions in fibroblast migration. *Mol. Biol. Cell.* 12:3947–3954.

Olbris, D. J., and J. Herzfeld. 1997. Variation of the rate of extension of actin networks. *In* Statistical Mechanics in Physics and Biology, Vol. 463. D. Wirtz and T. C. Halsey, editors. Pittsburgh Materials Research Society, Pittsburgh.

Oliver, T., M. Dembo, and K. Jacobson. 1999. Separation of propulsive and adhesive traction stresses in locomoting keratocytes. *J. Cell Biol.* 145:589–604.

Pantaloni, D., R. Boujemaa, D. Didry, P. Gounon, and M. F. Carlier. 2000. The Arp2/3 complex branches filament barbed ends: functional antagonism with capping proteins. *Nat. Cell Biol.* 2:385–391.

Pantaloni, D., and M. F. Carlier. 1993. How profilin promotes actin filament assembly in the presence of thymosin β4. *Cell.* 75:1007–1014.

Pantaloni, D., C. L. Clainche, and M. F. Carlier. 2001. Mechanism of actin-based motility. *Science.* 292:1502–1506.

Peskin, C., G. Odell, and G. Oster. 1993. Cellular motions and thermal fluctuations: the Brownian ratchet. *Biophys. J.* 65:316–324.

Petersen, N. O., W. B. McConnaughey, and E. Elson. 1982. Dependence of locally measured cell deformability on position of the cell, temperature and cytochalasin B. *Proc. Natl. Acad. Sci. U.S.A.* 79:5327–5331.

Pollard, T. D. 1986. Rate constants for the reactions of ATP- and ADP-actin with the ends of actin filaments. *J. Cell. Biol.* 103(6 pt 2): 2747–2754.

Pollard, T. D., L. Blanchoin, and R. D. Mullins. 2000. Molecular mechanisms controlling actin filament dynamics in nonmuscle cells. *Annu. Rev. Biophys. Biomol. Struct.* 29:545–576.

Raucher, D., and M. P. Sheetz. 1999. Membrane expansion increases endocytosis rate during mitosis. *J. Cell Biol.* 144:497–506.

Redmond, T., and S. H. Zigmond. 1993. Distribution of F-actin elongation sites in lysed polymorphonuclear leukocytes parallels the distribution of endogenous F-actin. *Cell Motil. Cytoskel.* 26:1–18.

Ressad, F., D. Didry, C. Egile, D. Pantaloni, and M. F. Carlier. 1999. Control of actin filament length and turnover by actin depolymerizing factor (ADF/Cofilin) in the presence of capping proteins and Arp2/3 complex. *J. Biol. Chem.* 274:20970–20976.

Ressad, F., D. Didry, G. X. Xia, Y. Hong, N. H. Chua, D. Pantaloni, and M. F. Carlier. 1998. Kinetic analysis of the interaction of actin-depolymerizing factor (ADF)/cofilin with G- and F-actin. *J. Biol. Chem.* 273:20894–20902.

Roberts, T., and M. Stewart. 2000. Acting like actin. The dynamics of the nematode major sperm protein (msp) cytoskeleton indicate a push-pull mechanism for amoeboid cell motility. *J. Cell Biol.* 149:7–12.

Rosenblatt, J., B. J. Agnew, H. Abe, J. R. Bamburg, and T. J. Mitchison. 1997. Xenopus actin depolymerizing factor/cofilin (XAC) is responsible for the turnover of actin filaments in *Listeria monocytogenes* tails. *J. Cell Biol.* 136:1323–1332.

Rotsch, C., K. Jacobson, and M. Radmacher. 1998. Dimensional and mechanical dynamics of active and stable edges in motile fibroblasts investigated by atomic force microscopy. *PNAS.* 96:921–926.

Roy, P., Z. Rajfur, D. Jones, G. Marriott, L. Loew, and K. Jacobson. 2001. Local photorelease of caged thymosin beta 4 in locomoting keratocytes causes cell turning. *J. Cell Biol.* 153:1035–1047.

Schafer, D. A., P. B. Jennings, and J. A. Cooper. 1996. Dynamics of capping protein and actin assembly in vitro: uncapping barbed ends by polyphosphoinositides. *J. Cell Biol.* 135:169–179.

Schwob, E., and R. P. Martin. 1992. New yeast actin-like gene required late in the cell cycle. *Nature.* 355:179–182.

Small, J. V., M. Herzog, and K. Anderson. 1995. Actin filament organization in the fish keratocyte lamellipodium. *J. Cell Biol.* 129:1275–1286.

Southwick, F. S. 2000. Gelsolin and ADF/cofilin enhance the actin dynamics of motile cells. *PNAS.* 97:6936–6938.

Svitkina, T. M., and G. G. Borisy. 1999. Arp2/3 complex and actin depolymerizing factor/cofilin in dendritic organization and treadmilling of actin filament array in lamellipodia. *J. Cell Biol.* 145:1009–1026.

Svitkina, T. M., A. B. Verhovsky, K. M. McQuade, and G. G. Borisy. 1997. Analysis of the actin-myosin II system in fish epidermal keratocytes: mechanism of cell body translocation. *J. Cell Biol.* 139: 397–415.

Theriot, J. A., and T. J. Mitchison. 1991. Actin microfilament dynamics in locomoting cells. *Nature.* 352:126–131.

Theriot, J. A., and T. J. Mitchison. 1992. Comparison of actin and cell surface dynamics in motile fibroblasts. *J. Cell Biol.* 119:367–377.

Theriot, J. A., T. J. Mitchison, L. G. Tilney, and D. A. Portnoy. 1992. The rate of actin-based motility of intracellular *Listeria monocytogenes* equals the rate of actin polymerization. *Nature.* 357:257–260.

Tilney, L. G., E. M. Bonder, and D. J. De Rosier. 1991. Actin filaments elongate from their membrane-associated ends. *J. Cell Biol.* 90: 485–494.

van Doorn, G. S., C. Tanase, B. M. Mulder, and M. Dogterom. 2000. On the stall force for growing microtubules. *Eur. Biophys. J.* 29:2–6.

Wang, Y. 1985. Exchange of actin subunits at the leading edge of living fibroblasts: possible role of treadmilling. *J. Cell Biol.* 101:597–602.

Wear, M. A., D. A. Schafer, and J. A. Cooper. 2000. Assembly and disassembly of actin networks. *Curr. Biol.* 10:R891–R895.